2024

Investigation of blood pressure waveform using harmonic distortion: implications for cardiovascular risk

BOSTON UNIVERSITY

COLLEGE OF ENGINEERING

Dissertation

INVESTIGATION OF BLOOD PRESSURE WAVEFORM USING HARMONIC DISTORTION: IMPLICATIONS FOR CARDIOVASCULAR RISK

by

NICHOLAS MILKOVICH

B.S., University of Virginia, 2018
B.A., University of Virginia, 2018
M.S., Boston University, 2021

Submitted in partial fulfillment of the

requirements for the degree of

Doctor of Philosophy

2024

Approved by

First Reader

Katherine Yanhang Zhang, Ph.D.
Professor of Mechanical Engineering
Professor of Biomedical Engineering
Professor of Materials Science and Engineering

Second Reader

Béla Suki, Ph.D.
Professor of Biomedical Engineering
Professor of Materials Science and Engineering

Third Reader

James Bird, Ph.D.
Professor of Mechanical Engineering
Professor of Materials Science and Engineering

Fourth Reader

Gary F. Mitchell, M.D.
President
Cardiovascular Engineering, Inc.
Norwood, Massachusetts

DEDICATION

For Xiaozhu Liu

ACKNOWLEDGMENTS

I would like to first thank my primary advisor, Professor Katherine Zhang, for her support and encouragement in these past years. Katherine has continuously encouraged me work hard and stay curious. I would also like to thank my co-advisor, Professor Bela Suki, who has been instrumental in developing the caliber of my work. The COVID-19 pandemic presented many challenges, and both my advisors were able to continue guiding me in spite of the unique circumstances. This dissertation would not be possible without their help.

I would also like to honorably thank my dissertation committee for their insightful advice and assistance through my education: Dr. R. Glynn Holt, Dr. James Bird, and Dr. Gary Mitchell, M.D. Thank you Dr. Francesca Seta for your collaboration.

To my father, Dr. Scott Milkovich, an endless thank you for keeping me sane and keeping my eyes on the prize. You are, and always will be, my favorite professor. To my mother, Leslie Mait, and my sister, Rachel Milkovich, I love you both with all my heart.

Additionally, I would like to thank my lab mates for our time working together: Xunjie Yu, Ruizhi Wang, Anastasia Gkousioudi, Songhao Li, Sam Halvorsen and Nick Ananchenko.

It is with a heavy heart that I also thank my late friend and lab mate, Xiaozhu Liu. Thank you for helping me with my homework so I could pass Continuum Mechanics. Thank you for sharing space with me all these years. Thank you for the small moments. Thank you for tolerating my jokes. Thank you for existing. I will never forget you and your kindness.

INVESTIGATION OF BLOOD PRESSURE WAVEFORM USING HARMONIC DISTORTION: IMPLICATIONS FOR CARDIOVASCULAR RISK

NICHOLAS MILKOVICH

Boston University College of Engineering, 2024

Major Professors: Katherine Yanhang Zhang, Ph.D., Professor of Mechanical Engineering, Professor of Biomedical Engineering, Professor of Materials Science and Engineering

and

Béla Suki, Ph.D., Professor of Biomedical Engineering, Professor of Materials Science and Engineering

ABSTRACT

Blood pressure waveform (BPW) can be used to characterize changes in the cardiovascular system due to diseases and aging. The BPW morphology is largely determined by both the total mechanical impedance of the vasculature and the flow waveform produced by the left ventricle. The BPW can be further decomposed into its two primary components: the forward and reflected waveforms. It is known that under several conditions, such as aging, arterial wall stiffening, and increased cardiovascular risk, the magnitudes and phases of these waves change and therefore distort the aggregate BPW. Previous studies of the BPW has yielded mixed results, largely due to the insensitivities of the primary wave morphology index, augmentation index (AI). To this end, a new method of morphology characterization was developed which takes into account the overall harmonic content of the BPW.

Harmonic distortion (HD), derived from Fourier-transformed BPW, was first used

to characterize changes in the aortic wall. Utilizing mice subjected to normal and high fat, high-sucrose diets, the results demonstrate that HD exhibits a linear relationship with both systolic blood pressure (SBP) and arterial stiffness. Next, a transmission line model of arterial impedance was developed to study physiologically realistic BPWs under various arterial tree sizes and stiffness. Comparison of HD and other indexes reveals that HD correlates strongly with arterial stiffness, surpassing AI in accuracy for higher stiffness values. Finally, HD analysis was applied to BPWs collected clinically on a diverse group of participants. HD emerges as a more sensitive indicator than AI, notably correlating with diabetes and demonstrating stability across heart rate variations. The superior statistical performance of HD over AI in hemodynamic variables underscores its potential as a robust measure for cardiovascular risk assessment. This research offers a comprehensive framework for assessing arterial health, highlighting the potential of HD as a stable, sensitive, and noninvasive measure. This integrated approach contributes to a nuanced understanding of the intricate factors influencing BPW morphology and its implications for cardiovascular health in the context of aging and disease.

TABLE OF CONTENTS

LIST OF TABLES

LIST OF FIGURES

CHAPTER 1 INTRODUCTION

1.1 Objectives

Arterial health crucially hinges on the elastic properties of the arterial wall, which play a pivotal role in maintaining optimal blood flow dynamics (Glasser et al., 1997; O'Rourke et al., 2016). In the presence of aging and cardiovascular diseases, such as diabetes mellitus (DM), heart failure, and stroke, the structural integrity of the arterial wall undergoes significant alterations, resulting in increased stiffness through a process known as arterial remodeling (Roman et al., 2000; Yambe et al., 2004; Rucka et al., 2015; O'Rourke et al., 2016). The pathological changes ultimately contribute to the development of hypertension (HT), a condition that carries substantial cardiovascular risks for affected individuals (Sun, 2015). Notably, cardiovascular diseases continue to rank as the foremost cause of mortality in developed nations, underscoring the pressing need for a deeper comprehension of arterial health changes under these pathological circumstances.

One avenue of investigation is the analysis of the blood pressure waveform (BPW) (Glasser et al., 1997; Kannel et al., 2003; Mitchell et al., 2004a; Bundy et al., 2017). By analyzing the various features and characteristics within BPWs, we can gain valuable insights into the differences between individuals afflicted with cardiovascular disease and aging-related arterial changes and those who are not. BPWs, essentially representations of blood pressure (BP) fluctuations over a brief temporal window, offer a straightforward, noninvasive means of assessment that can be readily incorporated into diverse clinical settings. The underlying aspiration is that by leveraging these waveforms

and conducting a meticulous assessment of the relative distortions they manifest, we can establish a straightforward and expedient method for evaluating arterial health.

This study delves into the potential of BPW analysis as a diagnostic tool for discerning and monitoring arterial function, particularly in the context of aging and cardiovascular conditions. We hypothesize that BPW can be used to derive indexes directly assessing arterial health in large elastic arteries. The overall goal of this study is to establish a relationship between BPW and arterial wall stiffness by unraveling the connection between arterial wall properties and hemodynamic blood flow. Through a comprehensive exploration of BPW features and their significance, we aim to shed light on the promise of this underutilized approach in contributing to our understanding of arterial health. First, we aim to develop and implement BPW analysis on waveforms collected from *in vivo* to assess BPW changes in a mouse model of diet-induced metabolic syndrome and aging. A new BPW index, harmonic distortion (HD), was introduced to quantify the energy in the BPW above the fundamental frequency. HD first uses a discrete Fourier transform of the BPW and then sums the magnitudes of the harmonics with respect to the fundamental frequency. Next, we developed a transmission line model to systematically study how hemodynamic flow and arterial wall mechanics contribute to BPW morphology, which was then assessed using the existing and newly developed BPW index. Last, we determined the efficacy of HD as an *in vivo* measurement of human tonometry BPWs collected by Framingham Heart Study (FHS).

1.2 Features of the blood pressure waveform

The BPW is predominantly composed of two interrelated wavelets (Figure 1.1), with the first being the forward-traveling wave, generated directly by the rhythmic contractions of the left ventricle of the heart. This wave emanates from the heart and courses through the intricate network of arterial branches within the circulatory system. As this blood flow progresses, it encounters peripheral resistance—a phenomenon arising from interactions with the arterial wall. The magnitude of this resistance is contingent upon both the material characteristics of the arterial wall and the fluid properties of the blood itself (Burattini et al., 1991; Wilkinson et al. 2002b; Hirata et al., 2006; Mitchell et al., 2008). Additionally, geometric attributes of the blood vessels, such as variations in vessel diameter and branching into smaller vessels, contribute to the overall impedance encountered by the forward-traveling wave (Westerhof et al., 2020). These combined factors contribute to the formation of an aggregate reflecting waveform, constituting the second wavelet within the comprehensive BPW (Figure 1.1).

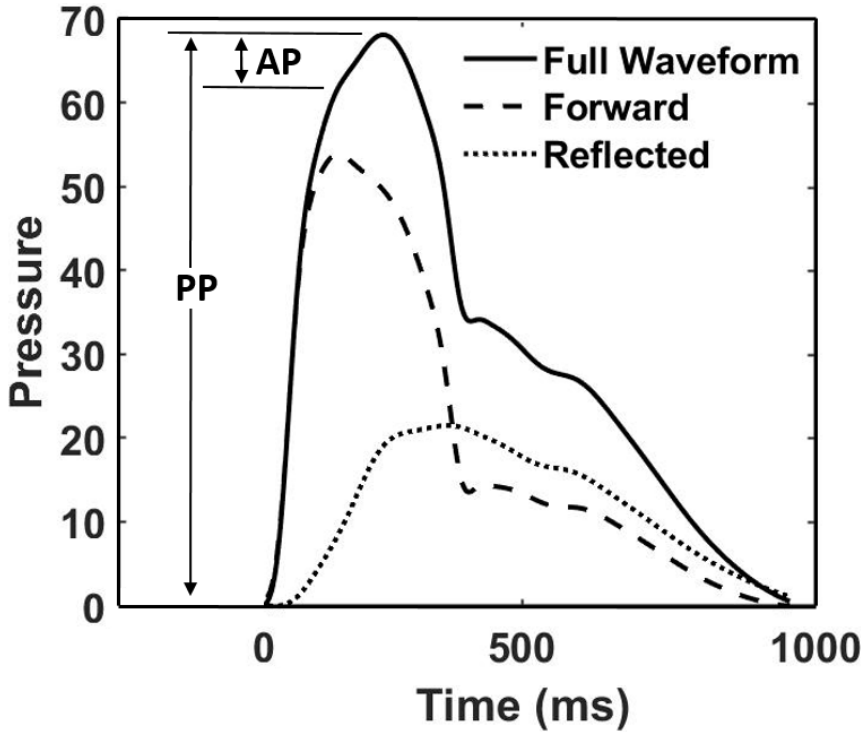

Figure 1.1: An illustrative representation of a generated blood pressure waveform, displaying its decomposition into two distinct wavelets: the forward and reflected waves. Additionally, the pressure values delineate the span over which pulse pressure (PP) and augmentation pressure (AP) are quantified.

It is worth noting that while multiple sources of waveform reflection exist within the arterial tree, research often simplifies the analysis by considering a single 'effective' reflection site when investigating wave reflections (Mitchell et al., 2004b; Davies et al., 2012). The dynamics of wave reflection, including transit time and magnitude, have been demonstrated to undergo alterations in various cardiovascular conditions (Wilkinson et al. 2002b; Hirata et al., 2006; Ageenkova et al., 2011; Mitchell et al., 2008). These changes in wave reflection characteristics have primarily been analyzed for their effects on augmenting the forward-traveling waveform, which has been the central focus of BPW feature analysis. However, these assessments have predominantly centered on the

magnitude of the reflection or other pressure ratios within the BPW, yielding limited and occasionally conflicting results (Hirata et al., 2006; Mitchell et al., 2008; Jerrard-Dunne et al., 2008; Ageenkova et al., 2011).

Pressure wave reflection within the arterial system serves two critical and beneficial purposes. Under normal conditions, the reflected wave returns to the central aorta during diastole, effectively bolstering diastolic perfusion pressure within the coronary circulation (Nichols and O'Rourke, 1998). Partial wave reflection also redirects a portion of the pulsatile energy carried by the waveform back to the central aorta, where it is subsequently dissipated through viscous damping. This mechanism serves to restrict the transmission of pulsatile BPW into the peripheral arterial system, mitigating the potential harm it might otherwise inflict upon the delicate microcirculation (Safar et al., 2003). The loss of this protective function associated with wave reflection holds the potential to contribute to the pathogenesis of an expanding spectrum of cardiovascular and noncardiovascular conditions associated with aging. These conditions, which share a potential microvascular etiology, encompass a range of ailments, including white matter lesions in the brain and renal dysfunction (Liao et al., 1997; Rizzoni et al., 2003; Safar et al., 2004; Mitchell et al., 2004a). Understanding the intricate role of wave reflection in these processes is imperative for advancing our comprehension of their underlying mechanisms and developing targeted interventions.

1.3 Outline of the research

In Chapter 1, we introduced the background, motivation and objectives of this study.

In Chapter 2, cardiovascular risk indices are introduced relating to both waveform morphology and waveform arrival times.

In Chapter 3 of our study, we delved into the examination of BPWs within a mouse model. To investigate the impact of dietary factors on arterial health, we employed two distinct diet regimens—normal diet and a high fat, high-sucrose diet designed to induce metabolic syndrome. These mice were closely monitored over an extended period, during which their blood pressure profiles were recorded. Following the monitoring period, the mice were humanely euthanized, and their carotid arteries were carefully extracted for subsequent mechanical testing. This allowed us to establish a crucial link between the HD of the in vivo-collected waveforms and the mechanical properties assessed in vitro, particularly arterial stiffness.

Chapter 4 of our research was dedicated to the development of a transmission line model that utilized electrical impedance as a substitution for mechanical impedance within the adult arterial tree. This comprehensive model accurately represented the material properties and geometric characteristics typical of an adult human, thereby enabling us to simulate input impedance across the entire arterial system. By systematically modulating parameters within a physiological range, we generated diverse BPWs within this model. Subsequently, we were able to establish a compelling connection between the HD values derived from these simulated human waveforms and

the estimated structural stiffness of the arterial system.

In Chapter 5, we transitioned to the application of our HD analysis in a human clinical study, conducted in collaboration with the Framingham Heart Study (FHS). In this clinical context, we examined BPWs collected noninvasively using over-the-skin tonometry. These valuable BPW datasets were augmented with additional clinical demographic information, as well as established indices like AI and PWV. The primary objectives of this chapter were twofold: firstly, to validate the utility of HD as a meaningful BPW index within a clinical setting, and secondly, to assess both its strengths and limitations when applied in real-world healthcare scenarios.

In Chapter 6, we summarize the conclusions in this study and present the outlook of future work.

CHAPTER 2 CARDIOVASCULAR RISK INDICES

2.1 Overview

This chapter presents BPW indices commonly used when assessing changes to the BPW and, by extension, arterial health. This includes Augmentation Index (AI), Reflection Magnitude (RM), and our proposed index Harmonic Distortion (HD), derived from BPW morphology. It also includes the gold standard of risk indexing, Pulse Wave Velocity (PWV).

2.2 Pulse wave velocity

PWV is widely considered to be the most accurate and reliable index of arterial stiffness (Wilkinson et al., 1998; Nichols 2005; Laurent et al., 2006). It has been used extensively in literature to quantify age-based arterial stiffening (McEniery et al., 2005) and has been seen to correlate strongly with cardiovascular diseases, such as: diabetes, hypertension, heart disease, stroke and further cardiovascular events (Blacher et al., 1999; Cruickshank et al., 2002; Meguro et al., 2009; Cecelja and Chowienczyk 2009; Weisbrod et al., 2013; Kim et al., 2014). Due to the strength of this index, it is often used to validate the efficacy of other cardiovascular risk indices (Mitchell et al., 2004).

PWV is calculated as the difference between arrival times of flow or pressure waveforms (Δt) over a length of artery:

$$PWV = \frac{L}{\Delta t} \tag{2.1}$$

where *L* represents the arterial region of interest, commonly across the carotid-femoral pathway to assess the health of the aorta (Figure 2.1) (Mitchell et al., 2004; Mitchell et al., 2010b). However, another common region is the carotid-radial or brachial-femoral pathways, which have been used to assess the health of muscular arteries (Mitchell et al., 2004; Mitchell et al., 2010b).

PWV measurements often require the use of specialized imaging devices that have not extensively infiltrated clinical practice, such as MRI and ultrasound machines (Vlachopoulos et al., 2015). Though PWV can be measured using less sophisticated means, for example: using direct measure of waveform transit times via cuff recordings at the ankle, thigh, finger or toe, these means are not often used for study or application in a clinical setting (Segers et al., 2020). Simplification of the technology and research into new inexpensive methods to measure or assess arterial health will facilitate its adoption in clinical practice.

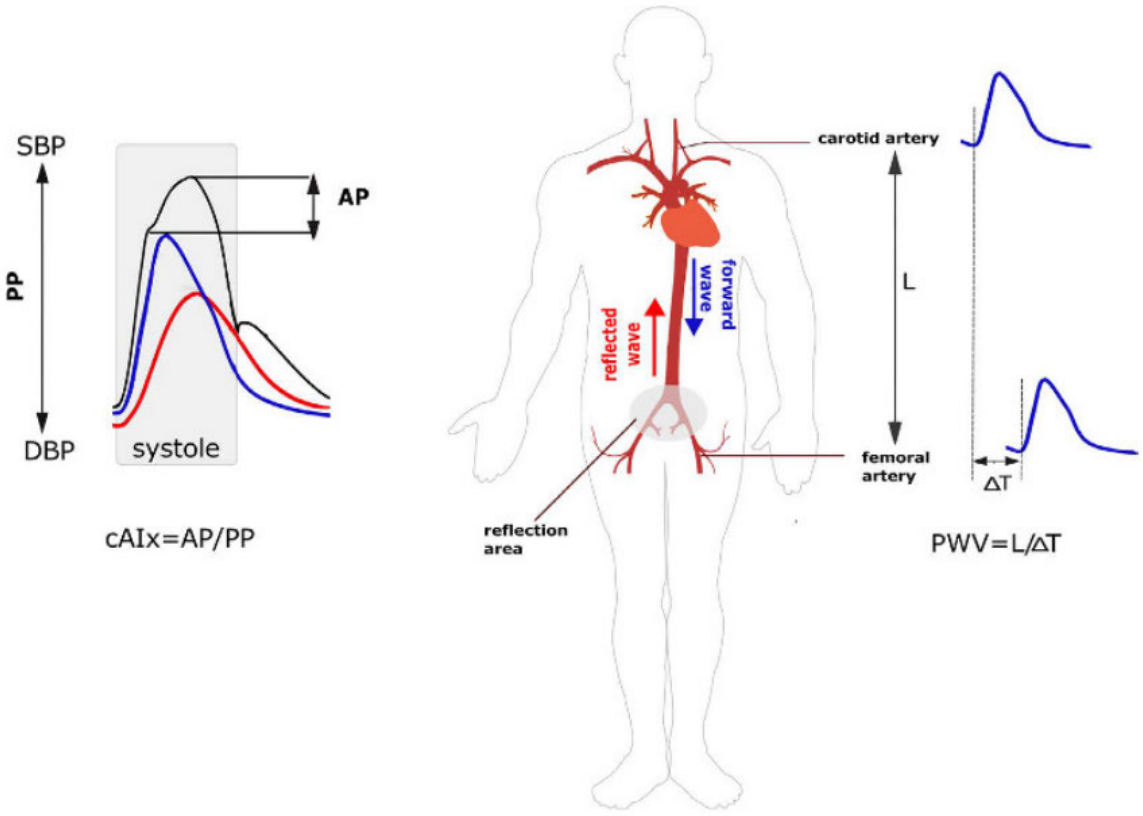

Figure 2.1: Schematic illustrating the regions of human vasculature in which pulse wave velocity and augmentation indices are calculated using waveform arrival times and waveform morphology, respectively. Jeroncic et al., 2016, *Sci. Reports*

2.3 Morphology indices

2.3.1 Augmentation index

AI stands out as the most widely employed metric for assessing wave reflection within the context of BPWs (Wilkinson et al., 2002b; Ayer et al., 2010). It is derived by computing the ratio between the augmentation pressure (AP) and the pulse pressure (PP) (Figure 1.1 and Figure 2.1) and the equation:

$$AI = \frac{AP}{PP} \tag{2.2}$$

Determining these specific BPW features entails the identification of the inflection point on the upstroke, a point that demarcates the convergence of the two constituent wavelets within the BPW.

Initially, AI was investigated as a potential parameter capable of directly quantifying arterial stiffness. However, a series of studies have unveiled results marked by inconsistency and modest correlations when compared to the gold-standard measurement of arterial stiffness, namely PWV (Lacy and Williams 2005; Sakurai et al., 2007; Mitchell 2008). One notable limitation of AI in serving as an index for evaluating arterial health is its characteristic decline beyond the age of 60 (Mitchell et al., 2004). This decline is attributed to the interplay between muscular arteries, which continue to undergo stiffening, and elastic arteries, which maintain a relatively stable PWV despite the aging process (Mitchell et al., 2010b).

The declining trend of AI with advancing age beyond the 60-year mark underscores the need for a more nuanced understanding of arterial health and the impact of aging on different components of the arterial system. While AI remains a valuable tool for assessing wave reflection, its limitations in capturing the full spectrum of arterial health dynamics necessitate a more comprehensive approach that considers the multifaceted nature of arterial changes with age. In this context, the exploration of alternative indices and complementary measures may provide a more holistic perspective on arterial health and its intricate relationship with aging and other cardiovascular factors.

2.3.2 Reflection magnitude

RM represents a straightforward assessment of the pressure magnitude associated with the reflected wave, a value determined through the decomposition of the aggregate BPW into its constituent wavelets using the flow waveform (Mitchell, 2008; Mitchell et al., 2008; Mitchell et al., 2010b). Figure 1.1 and Figure 2.1 illustrate this waveform decomposition and RM is simply the magnitude of the reflected wave. Notably, RM exhibits a robust correlation with the AI, a widely utilized metric for wave reflection evaluation (Segers et al., 2007a). However, despite this correlation, RM fails to meet the established criteria that define AI and consequently does not emerge as a favored alternative to this measure.

While RM offers valuable insights into the pressure magnitude of the reflected wave, its shortcomings become apparent when considering the specific limitations set by AI. AI's comprehensive approach, which encompasses both augmentation pressure and pulse pressure, provides a more holistic perspective on wave reflection and arterial health. In contrast, RM's singular focus on the pressure magnitude of the reflected wave lacks the broader context provided by AI. Consequently, RM may not capture the intricacies of wave reflection dynamics and arterial health as comprehensively as AI, making it less suitable as a direct replacement for this established metric.

2.4 Harmonic distortion

2.4.1 Index calculation

To quantitatively compare BPWs, we introduce an index, HD that will be used to quantify the shape change of BPW (Milkovich et al., 2022). HD is defined based on the discrete Fourier transform (DFT) of the BPW, as:

$$HD = \frac{\sum_{k=2}^{F} |A_k|^2}{|A_1|^2} \tag{2.3}$$

where $|A_k|^2$ are the Fourier coefficients of a single BPW multiplied by their complex conjugates. HD thus represents the ratio of energy above the fundamental frequency to that at the fundamental frequency of the waveform. Here, Fourier coefficients higher than F were assumed negligible since they did not significantly contribute to the HD value. F differs by the type of waveform being analyzed, mouse (F = 7) or human (F = 20), due to fundamental frequency and heart rate differences.

For an ideal sinusoidal wave, the HD value is 0. As an illustration, the normalized power spectrum, $\frac{|A_k|^2}{|A_1|^2}$, were obtained for a triangle wave and a mouse BPW (Figure 2.2a) using a custom MATLAB code according to Equation 2.3 and plotted in Figure 2.2b. The triangle wave has a HD value of 0.014 whereas the sample BPW waveform is more distorted with an HD value of 0.025.

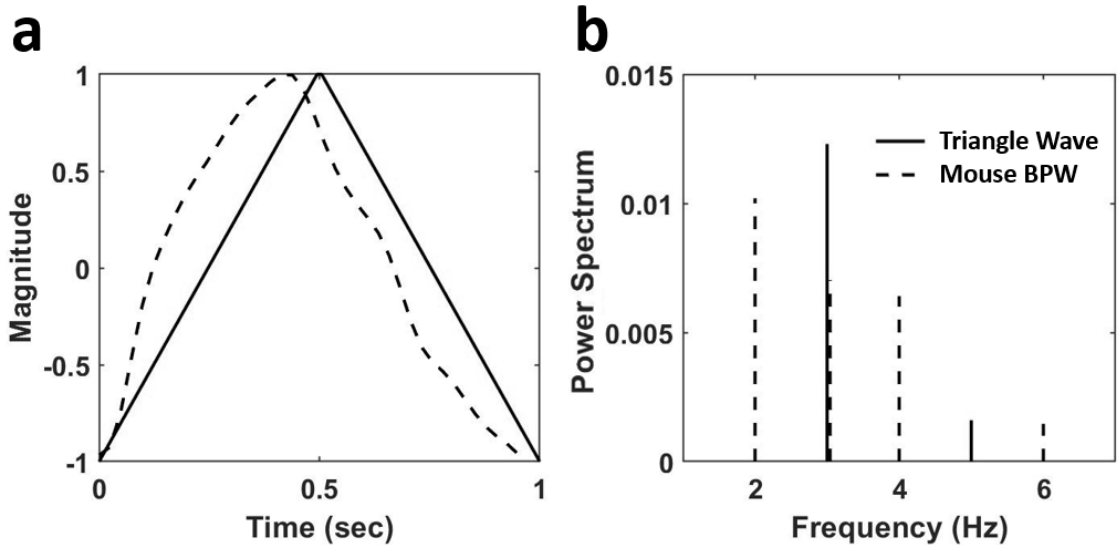

Figure 2.2: (a) A triangular wave (solid line) and a normalized BPW from radiotelemetry (dashed line. (b) The normalized power spectrum, calculated as the squared fraction of Fourier coefficients at higher frequencies to the fundamental frequency of the waveforms in (a) at 1 Hz.

2.4.2 Index overview

The harmonic distortion (HD) index aims to provide a means of analyzing BPW without necessitating waveform decomposition or inflection point detection, as is typically required by the two previously discussed indices, AI and RM. (Milkovich et al., 2022). This method was first introduced to biological waveforms when used to assess the harmonics of respiratory cycles (Zhang et al., 1995). This innovation holds the promise of simplifying waveform analysis significantly. The computation of this index involves a transformation of the BPW into the frequency domain. Subsequently, it quantifies the cumulative energy of higher order harmonics in relation to the fundamental frequency of the waveform, essentially representing the energy content above the fundamental frequency (Milkovich et al., 2022).

In the course of our research, we have noted a notable characteristic of HD — its propensity to converge toward zero as individuals age (Figure 2.4) (Milkovich et al., 2022). Additionally, HD exhibits sensitivity to various other measures, including tangent stiffness, PWV, structural stiffness, and the presence of diabetes (Milkovich et al., 2022). This versatility underscores the potential of the HD index as a robust tool for assessing arterial health and its responsiveness to a spectrum of cardiovascular parameters.

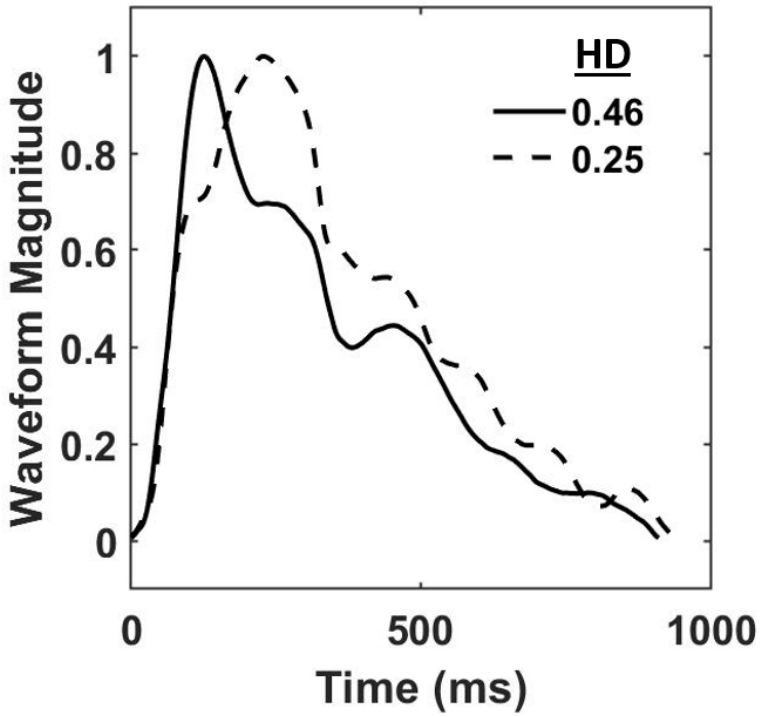

Figure 2.3: BPWs from 21 and 51 y/o normotensive human female participants, respectively, with blood pressure normalized between 0 and 1 to illustrate the movement of wave reflection under age-based arterial changes. These changes are quantified by HD, a BPW index.

The HD index analysis is easily implemented in diverse subject contexts, including studies involving both mice and humans (Figure 2.4), as well as the analysis of waveforms simulated using a custom transmission line model. This versatility positions

HD as a valuable addition to the toolkit of researchers and clinicians seeking to gain insights into arterial health and its associations with various physiological and pathological factors across different populations and experimental settings.

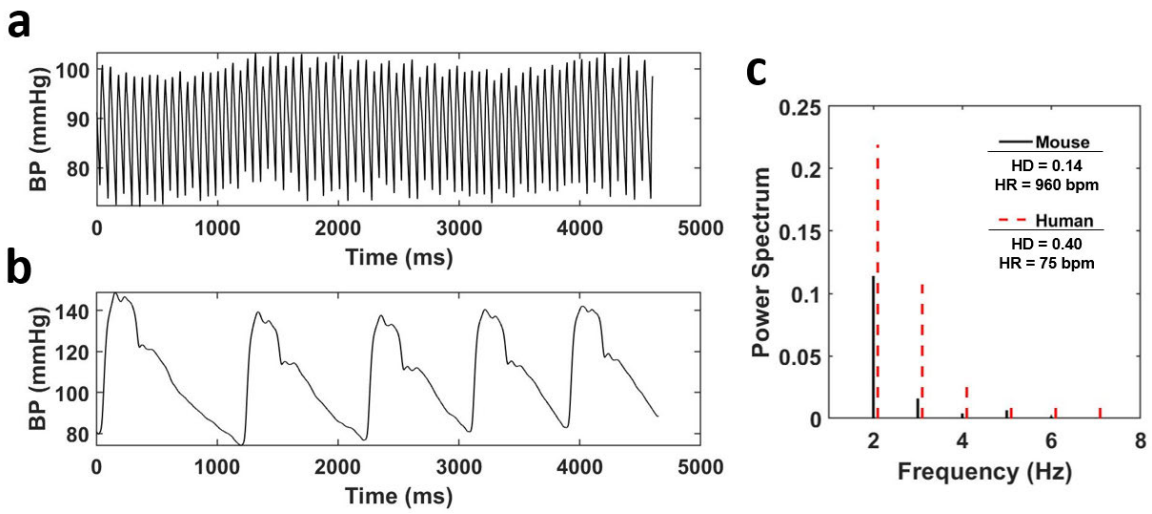

Figure 2.4 A 4.6 second BPW sample collected from the common carotid artery of (a) a mouse aged 6 months, male, fed on a normal diet schedule and (b) a normotensive human male, 46 years of age with their power spectrum (c) plotted up to 8 Hz The mouse waveform was recorded using a catheter surgically implanted directly in at the top of the aortic arch via the right carotid artery and measured with radiotelemetry. The human waveform was recorded by a technician using over the skin tonometry above the carotid artery.

CHAPTER 3 HARMONIC DISTORTION OF BLOOD PRESSURE WAVEFORM AS A MEASURE OF ARTERIAL STIFFNESS

3.1 Overview

Aging and disease alter the composition and elastic properties of the aortic wall resulting in shape changes in blood pressure waveform (BPW). Here, we propose a new index, harmonic distortion (HD), to characterize BPW and its relationship with other in vitro and in vivo measures. Using a Fourier transform of the BPW, HD is calculated as the ratio of energy above the fundamental frequency to that at the fundamental frequency. Male mice fed either a normal diet (ND) or a high fat, high sucrose (HFHS) diet for 2–10 months were used to study BPWs in diet-induced metabolic syndrome. BPWs were recorded for 20 s hourly for 24 h, using radiotelemetry. Pulse wave velocity (PWV), an in vivo measure of arterial stiffness, was measured in the abdominal aorta via ultrasound sonography. Common carotid arteries were excised from a subset of mice to determine the tangent modulus using biaxial tension-inflation test. Over a 24-h period, both HD and systolic blood pressure (SBP) show a large variability, however HD linearly decreases with increasing SBP. HD is also linearly related to tangent modulus and PWV with slopes significantly different between the two diet groups. Overall, our study suggests that HD is sensitive to changes in blood pressure and arterial stiffness and has a potential to be used as a noninvasive measure of arterial stiffness in aging and disease.

3.2 Introduction

Arterial stiffening is a significant contributor to the progression of cardiovascular diseases, including hypertension, diabetes mellitus, stroke, heart failure, and renal failure, which are the leading cause of mortality in the developed countries (Roman et al., 2000; Yambe et al., 2004; Rucka et al., 2015; O'Rourke et al., 2016). Arteries gradually stiffen with aging, which can lead to hypertension (HT) (Sun, 2015). Diabetic patients, however, show accelerated arterial stiffening with elevated blood pressure (BP) at a relatively young age compared to nondiabetic subjects (Chaturvedi, 2007; Loehr et al., 2016). BP is routinely used as a critical clinical measure for the diagnosis of HT. Additional parameters derived from BP and artery dimensions, such as distensibility and compliance, have been widely used both in clinics and research as indicators of the mechanical properties of arteries (Glasser et al., 1997; Kannel et al., 2003; Bundy et al., 2017). However, these parameters solely rely on the systolic, mean, and diastolic pressure values, and the inherent biomechanical information associated with the shape of the BP waveform (BPW) is not considered. For example, there is a marked difference in BPW in central aortic pressure as well as pressure measured in upper limb arteries between young and older individuals due to wave reflection (Hirata et al., 2006). Arterial stiffening results in a pressure augmentation from the superposition of the propagating and reflected waves, which increases the peak of the waveform in the systolic phase of the cardiac cycle (van Varik et al., 2012). Therefore, the features of BPW are associated with arterial stiffness; however, the phenomenon is compounded by the nonlinear elastic behavior of the vascular wall and how pathologic changes in wall properties contribute to changes in

BPW shape are not well understood.

The BPW is composed of a propagating wave, generated by cardiac contraction, and a reflected wave, from peripheral vessels to the proximal aorta. In clinical practice, indexes based on BPW are limited by their sole use of pressure differences (systolic minus diastolic) based on blood pressure measurements done on peripheral arteries (brachial arteries). One of the most widely used parameters, augmentation index (AI), quantifies the difference in pressure between the propagating wave and the reflected wave. Studies that sought to link AI to arterial stiffening and HT have shown that AI and pulse wave velocity (PWV), the gold standard clinical measure of arterial stiffness (Blacher et al., 1999; Nichols, 2005), are correlated with age, height, SBP, cholesterol and pulse pressure (Blacher et al., 1999; Brooks et al., 1999; Wilkinson et al., 2000; Brooks et al., 2001; Wilkinson et al., 2002b; Nichols, 2005). Interestingly, AI and PWV were not strongly correlated with one another (Jerrard-Dunne et al., 2008). Females tend to have higher AI, an effect that seems to be independent from height and heart rate (Hayward and Kelly, 1997; Gatzka et al., 2001; Mitchell et al., 2010b). This sex dependence of AI is present since prepuberty. Elevated AI is present in young girls (age 8.0 ± 0.1 years) compared to males of the same age, independent of factors that generally result in earlier wave reflection and increased AI, such as height or arterial stiffness (Ayer et al., 2010). Another BP index, reflection magnitude, is measured as the relative pressure magnitude of the reflected wave compared to the forward wave, which was suggested to better represent the overall changes due to the reflected wave (Mitchell,

2008; Mitchell et al., 2008; Mitchell et al., 2010b). However, the correlation between reflection magnitude and AI is less than 0.6 (Segers et al., 2007a). Additionally, both fail to assess changes in the waveform beyond a simple increase in pressure, neglecting BPW features such as the time delay between the forward and reflected wave, which may also change the overall shape of the BPW (Ageenkova and Purygina, 2011; Theodor et al., 2014).

In this study, we aim to establish a relationship between BPW and arterial wall stiffness to understand the complex interplay between hemodynamic flow and the nonlinear mechanical properties of the arterial wall and how they manifest in BPW. To this end, we introduced a new index characterizing BPW, harmonic distortion (HD), which we hypothesize will provide a more comprehensive assessment of the BPW. A mouse model of diet-induced metabolic syndrome was used to validate the effectiveness and applicability of this new index. The BPW, collected using radiotelemetry, were analyzed for two diet groups. HD based on spectral analysis of the BPW was obtained and used to quantify the distortion of the BPW and compared to established stiffness indexes.

3.3 Material and methods

3.3.1 Animal model

All procedures were approved by the Boston University Institutional Animal Care and Use Committee. Male (n = 29) C57Bl/6J mice were purchased from the Jackson Laboratory (Bar Harbor, ME, United States) at 7 weeks of age. After 1 week of acclimation, the 2-month-old (-mo) mice were fed a control normal diet (ND: 4.5% fat, 0% sucrose, catalog number D09071702, Research Diets, New Brunswick, NJ, United States) or high fat, high sucrose diet (HFHS: 35.5% fat, 16.4% sucrose) ad libitum (catalog numbers D09071703, Research Diets, New Brunswick, NJ, United States). In this model of diet-induced metabolic syndrome, mice develop hyperinsulinemia, glucose intolerance, increased arterial stiffness and hypertension within 8 months on diet, closely mimicking the human metabolic syndrome, as previously described (Weisbrod et al., 2013). Mice were kept in 12 h light/dark cycles in temperature- and humidity-controlled rooms. Briefly, mice were kept anesthetized (1–2% isofluorane) on a heating pad (Figure 3.1), while a gel-filled pressure catheter was carefully inserted in the aortic arch via catheterization of the left carotid artery. Therefore, all BPW measurements made with radiotelemetry are local to the aortic arch and indicative of central pressure.

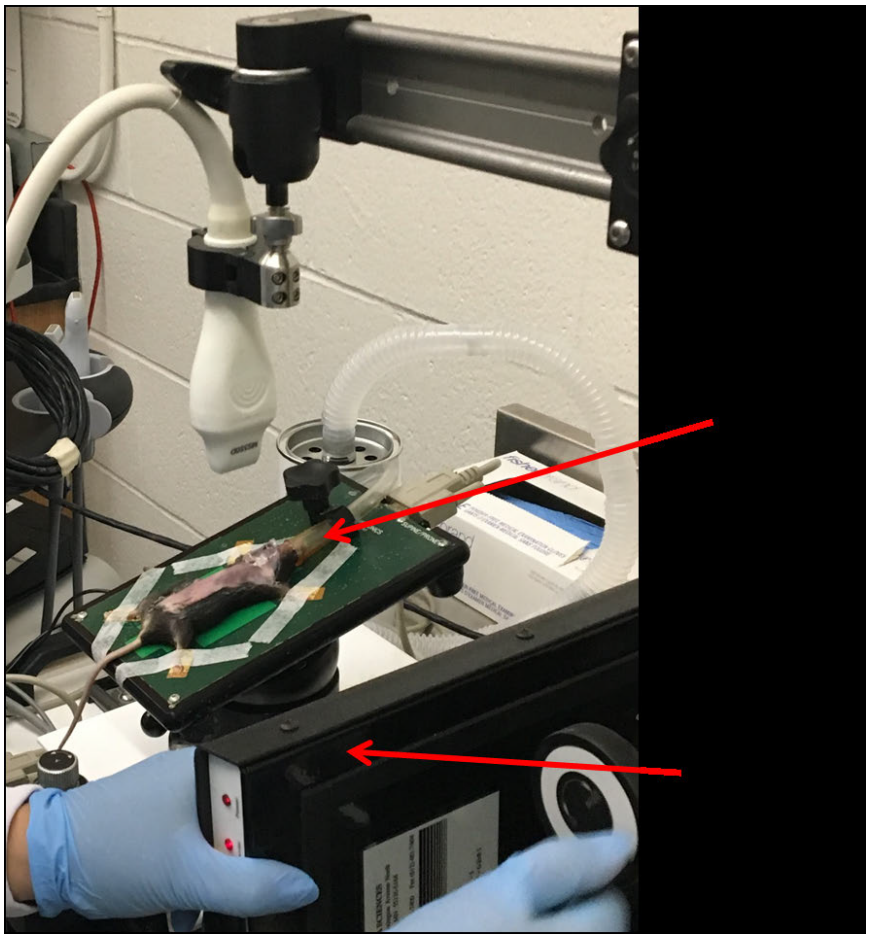

Figure 3.1: Image of anesthetized mouse specimen shaved from surgery with radio sensor in proximity to the specimen's radiotelemetry for blood pressure waveform collection.

After recovery from surgery (1–2 weeks), BPW recordings were acquired for 20 seconds hourly over a 24-hour period in the conscious, freely moving mice. BPWs are collected wirelessly through an external receiver and a data processing matrix (Figure 3.1). Mice were divided into subsets for various experimental conditions. One subset of mice (n = 6) had baseline BPW measurements taken at 2-months, before initiation of the HFHS diet, and subsequently fed the HFHS with measurements taken longitudinally at 3- and 4-months. A second subset of mice (ND: n = 5, HFHS: n = 8) underwent

radiotelemetry implantation procedures at 6-months and had BPW measurements taken at 8- and 10-months. A third subset of mice were fed ND (n = 6) or HFHS (n = 4) and euthanized at 4- and 10-months for in vitro mechanical analysis of their right carotid arteries.

3.3.2 In vivo blood pressure measurements

The BPW was measured using radiotelemetry (Data Sciences International, St Paul, MI, United States) that was implanted following standard surgical procedures, as we previously described (Weisbrod et al., 2013). Briefly, mice were kept anesthetized (1–2% isofluorane) on a heating pad, while a gel-filled pressure catheter was carefully inserted in the aortic arch via catheterization of the left carotid artery (Figure 3.2a).

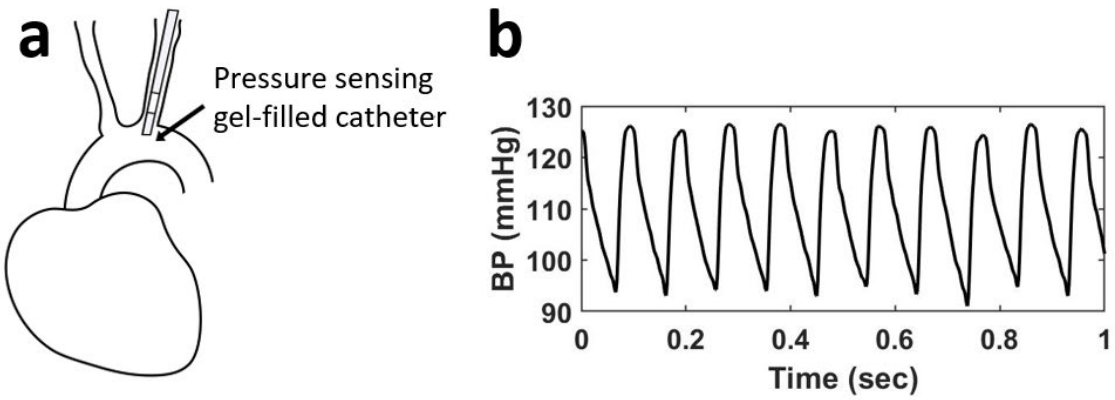

Figure 3.2: (a) A gel-filled pressure catheter is surgically inserted in the left common carotid artery of a mouse, with the pressure-sensing region (4 mm) resting in the aortic arch. (b) Example of *in vivo* BPWs over 1 second time period measured using radiotelemetry.

Therefore, all BPW measurements made with radiotelemetry are local to the aortic arch and indicative of central pressure. After recovery from surgery (1–2 weeks),

BPW recordings were acquired for 20 s hourly over a 24-h period in the conscious, freely moving mice. BPWs are collected wirelessly through an external receiver and a data processing matrix (Figure 3.2a). This resulted in a total of 24 distinct recordings for each mouse, with each recording consisting of many individual waveforms (Figure 3.2b). The SBP values from each waveform were then collected and separated into 16 blood pressure bins, ranging from 80–180 mmHg, for clarity of group overlap. Normalized probability density distributions of the average SBP of each bin was then generated for every mouse. The distributions were then fitted with Gaussian functions using a MATLAB program.

For HD analysis of the BPW, waveforms corresponding to a single heartbeat were isolated using custom MATLAB code by identifying the diastolic BPs. Equation 2.3 was then used to determine the HD value for each individual waveform. This analysis was performed on all mice and for all 24 BPW recordings. The corresponding SBP, the maximum value of BP in an isolated individual waveform, was also recorded and 12 evenly spaced BP bins were created between the minimum and maximum SBP values. The bin size was chosen by studying multiple bin sizes and assessing their effect on the slope of the regression line. Because the bins are weighted, the slope of these regressions is not sensitive to bin sizes. Hence, the bin size was kept consistent for all mice. The mean and standard deviation (SD) of HD corresponding to each BP bin were calculated. HD values that were two SD outside of the mean HD value were removed. The mean and SD of HD were then recalculated for each BP bin as well as the corresponding mean BP,

resulting in 12 data points for each mouse. A weighted linear regression between the mean HD and the mean BP was performed for each age and diet group. The weight of each data point was determined by the ratio of the number of HD values in the BP bin to the total number of HD values recorded for the mouse.

3.3.3 Pulse wave velocity measurements

Blood flow waves at two locations along the abdominal aorta, one proximal and one distal to the heart, using the renal artery as anatomical reference, were obtained in each age and diet group using high-resolution Doppler ultrasound (Vevo2100, Fujifilm Visualsonics, Toronto, ON, Canada), as we previously described (Weisbrod et al., 2013). PWV, the rate at which BP waves travel along the aorta, was calculated as the ratio of the distance between the two locations and the difference in arrival times of two consecutive flow waves, using the foot-to-foot method and the ECG as fiducial point, over 5–10 cardiac cycles for each mouse.

3.3.4 Biaxial inflation-extension test

To characterize the mechanical response of mouse carotid arteries, segments of artery about 6 mm in length were tested on a pressure myograph (110P DMT, Danish Myo Technology, Denmark) which allows the intraluminal pressure and axial force to be measured during the testing (Figure 3.3).

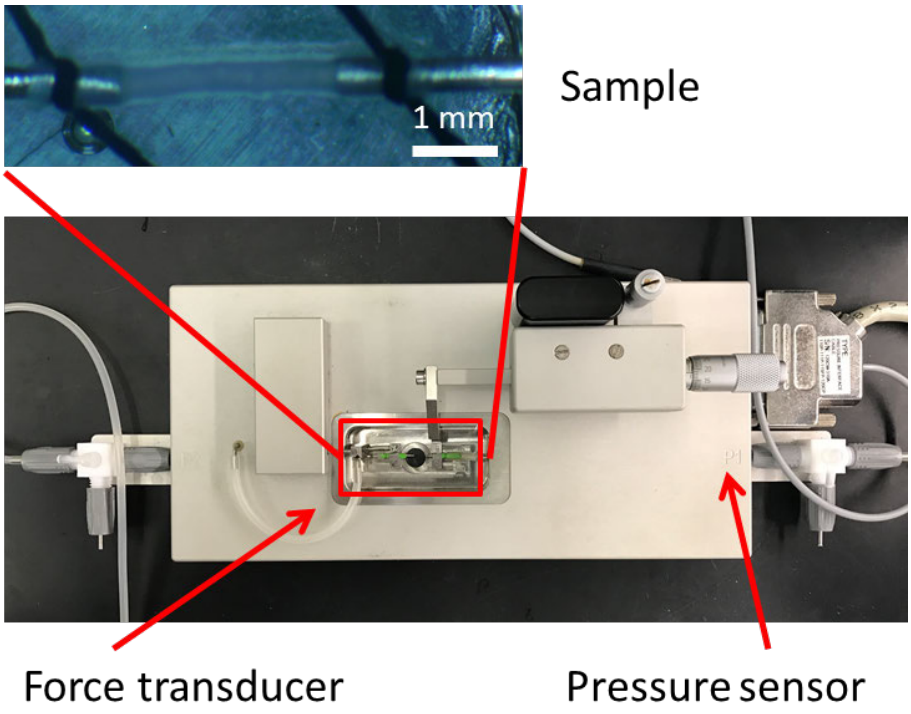

Figure 3.3: Picture of the pressure-diameter tester showing the sample cannulated on the stainless steel cannulas with sutures.

Arteries were carefully cleaned from surrounding fat and connective tissue and stored in phosphate buffered saline (PBS) at room temperature (22° C) until mechanical testing, which was performed within 12 hours of dissection (Mitchell et al., 2009). Briefly, each artery was cannulated in a pressure myograph and secured using a 7-0 suture. During testing, arteries were immersed into PBS at 22ºC. Arteries were then stretched to an axial stretch ratio (λ_z) of 1.8 and preconditioned with 3 cycles of inflation from 0 to 140 mmHg. After preconditioning, the *in vivo* value of λ_z was estimated by inflating each artery at a pressure of 50, 90 and 120 mmHg and axially stretching it at each pressure from λ_z = 1 to λ_z = 2 with 0.1 increments. The *in vivo* stretch ratio is identified as the intersection point of the three axial stretch-axial force curves.

Next, pressure-diameter tests were performed at and 5% above and below the estimated *in vivo* stretch ratio (λ_z^{iv}, λ_z^+ and λ_z^-). The loading protocol consisted of one cycle of a stepwise inflation and deflation of the artery at each axial stretch ratio from 0 to 140 mmHg with 10 mmHg increments and a loading rate of 5 mmHg/sec. The axial force, outer diameter, as well as the applied pressure were recorded throughout the mechanical testing. After mechanical testing, arterial rings of ~0.5 mm length were cut and imaged under an optical microscope. Images were imported into FIJI (http:/Fiji.sc/Fiji, Ashburn, VA). Outer and inner circumference were manually traced in order to calculate the corresponding unloaded diameters. Under thin wall assumption, Cauchy stresses in the circumferential and longitudinal directions can be calculated as (Ferruzzi et al., 2013; Gkousioudi et al., 2022):

$$\sigma_\theta = \frac{Pr_i}{h} \quad \text{and} \quad \sigma_z = \frac{f + P\pi r_i}{\pi h(2r_i + h)} \tag{3.1}$$

where P is the transmural pressure, f is the axial force, r_i is the deformed inner radius and h is the deformed thickness. With incompressibility assumption, the deformed inner radius can be calculated as (Ferruzzi et al., 2013; Gkousioudi et al., 2022):

$$r_i = \frac{1}{2}\sqrt{d_o^2 - \frac{D_o^2 - D_i^2}{\lambda_z}} \tag{3.2}$$

where d_o is the deformed outer diameter, λ_z the axial stretch ratio and D_o and D_i are the undeformed outer and inner diameter, respectively.

3.3.5 In vitro determination of tangent modulus

To establish the relationship between HD and arterial stiffness, tangent modulus of the common carotid arteries was obtained from a subset of mice from the 4-months ND (n = 3), 4-months HFHS (n = 2), 10-months ND (n = 3) and 10-months HFHS (n = 2) groups. Biomechanical characterization of these arteries was performed in a separate study by Gkousioudi et al., 2022, from which the circumferential Cauchy stress-stretch responses were obtained from biaxial extension-inflation tests, and then fitted using a four-fiber family constitutive model with the following strain energy function (Ferruzzi et al., 2013; Ferruzzi et al., 2018a):

$$W(\boldsymbol{C}, \boldsymbol{a}^i) = \frac{c}{2}(I_C - 3) + \sum_{i=1}^{4} \frac{c_1^i}{c_2^i}\left\{exp\left[c_2^i\left(I_4^i - 1\right)^2\right] - 1\right\} \tag{3.3}$$

In this constitutive model, arterial wall is considered a composite of the isotropic extracellular matrix (elastic fibers, cells and ground substance) and anisotropic collagen fibers, which are assumed to be oriented in four directions: axial ($\varphi^1 = 0^o$), circumferential ($\varphi^2 = 90^o$), and diagonal ($\varphi^3 = -\varphi^4 = \varphi$). c and $c_{1,2}^i$ are material parameters for the isotropic matrix and the collagen fibers, respectively. $\boldsymbol{C} = \boldsymbol{F}^T\boldsymbol{F}$ is the Cauchy-Green deformation tensor with $\boldsymbol{F}$ being the deformation gradient. $I_C = tr\boldsymbol{C}$ is the first invariant of $\boldsymbol{C}$. $I_4^i = \boldsymbol{a}^i \cdot \boldsymbol{C}\boldsymbol{a}^i$ represents the invariant that is associated with the i^{th} fiber family, and $\boldsymbol{a}^i$ is the unit vector that denotes the orientation of the i^{th} fiber family. In this study, circumferential tangent modulus, Cθθθθ, was calculated as the first derivative of the Cauchy stress-stretch expressions using the best-fitted model parameter

values as (Baek et al., 2007; Gkousioudi et al., 2022):

$$C_{\theta\theta\theta\theta} = 2t_{\theta\theta} + 4\lambda_\theta^4 \left(\frac{\partial^2 W}{\partial \lambda_\theta^2 \partial \lambda_\theta^2} + 2\sin^4 a_o \frac{\partial^2 W}{\partial \lambda_\theta^2 \partial \lambda_\theta^2} \right) \tag{3.4}$$

where $t_{\theta\theta}$ is the Cauchy stress in the circumferential direction, λ_θ is the circumferential stretch, W is the strain energy function based on the four-fiber family constitutive model, and a_o is the orientation angle of the diagonal collagen fiber families with respect to the longitudinal direction, and it was estimated during nonlinear regression model fitting (Ferruzzi et al., 2013; Ferruzzi et al., 2018a; Gkousioudi et al., 2022). Tangent modulus, $C_{\theta\theta\theta\theta}$, was then calculated as a function of the circumferential stretch λ_θ.

To establish a proper relationship between the HD obtained from in vivo measurements and the tangent modulus from the in vitro measurements, perivascular pressure, the pressure difference between the luminal and transmural pressures (Goshy et al., 1979; Kim et al., 2013; Ferruzzi et al., 2018b), needs to be considered to obtain the in vivo transmural pressure. Here, an estimation of average perivascular pressure 13.22 mmHg was obtained by incrementally adjusting its value for the best linear regression fit between HD and tangent modulus for each mouse. This average perivascular pressure value was then subtracted from the in vivo luminal SBP of each mouse to obtain transmural SBP.

3.3.6 Statistical analysis

Wilcoxon rank sum tests were performed on the low and high SBP means of each mouse group after normality was not found using one-sample Kolmogorov-Smirnov tests. HD values for each mouse group were found to be not normally distributed using paired Kolmogorov-Smirnov tests. Therefore, Friedman tests were performed on HD values between mouse groups when groups had the same number of subjects and Skillings-Mack tests were performed when comparing groups with a different number of subjects. A p-value of 0.05 or lower was considered statistically significant.

3.4 Results

3.4.1 Blood pressure variability

BPW data were firstly used to assess the variation of BP over a 24-h period. Probability density distributions of the SBP, i.e., the peak of the individual BPWs, were plotted for each mouse. Figure 3.4a shows a typical bimodal distribution of the SBP over a 24-h period. The data were fit with the sum of two Gaussian distributions with each peak centering at a low and high systolic blood pressure. The low- and high-pressure values at the two peaks were averaged for each age and diet group. The SBP distribution of the HFHS mouse showed a wider range of high SBP compared to the ND mouse with the two peaks correlating with age and diet. There was a significant increase in the SBP means with age in the ND groups (Figures 3.4b Figure 3.4c), however this trend was absent in the HFHS groups. The 2-months ND group's mean low- and high-pressure

values are statistically lower than all other groups, except the 4-months HFHS and the 3-months HFHS high pressure mean.

In the current study, 5 of the 19 analyzed BPW were found to either have one or three modes (n = 2 and 3, respectively). The single mode's mean corresponded to the group high pressure average and was included as such. In the three modes case, a mean value of either high or low pressure was only included if the Gaussian distribution could be fitted to the pressure distribution, and the mode with a mean outside of one standard deviation of the low or high mean was discarded.

3.4.2 Harmonic distortion

HD analysis showed that the HD values from the isolated individual BPW were inversely related to SBP over a 24-h period, as shown in Figure 3.5a for an 8-months ND mouse. The HD values range from ~0.24 to 0.03 between SBP of 93 and 153 mmHg. To study the trend between HD and SBP, evenly spaced blood pressure bins were used to find a mean HD within each bin. This mean HD is then plotted with the mean SBP of that bin for every mouse. Despite the large spread of HD seen in Figure 3.5a, following binning, a linear relation was apparent as shown for the 8-months ND group in Figure 3.4b.

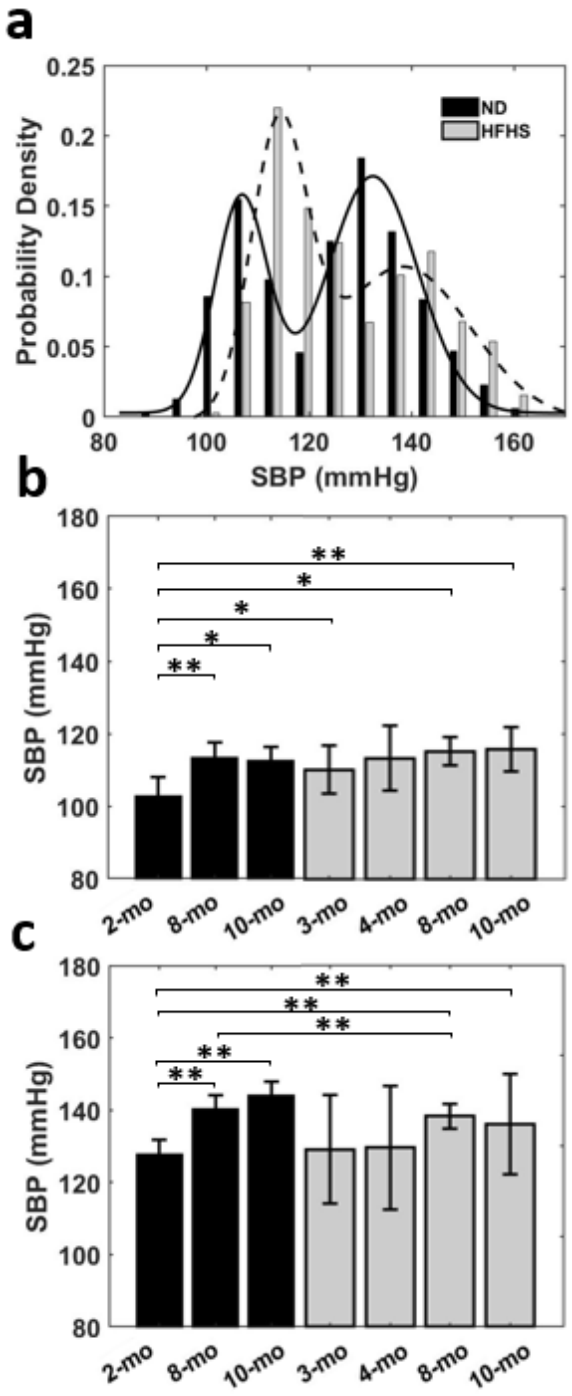

Figure 3.4: (a) Representative bimodal probability density distribution of SBP over a 24-h period for a 2-months ND and a 3-months HFHS mouse. Solid and dashed lines are Gaussian distributions fit to the data. The low- and high-pressure values of the bimodal SBP distribution for each age and diet groups were averaged and showed in (b,c) for the low and high pressure means, respectively, for the age and diet groups (*p < 0.05; **p < 0.01).

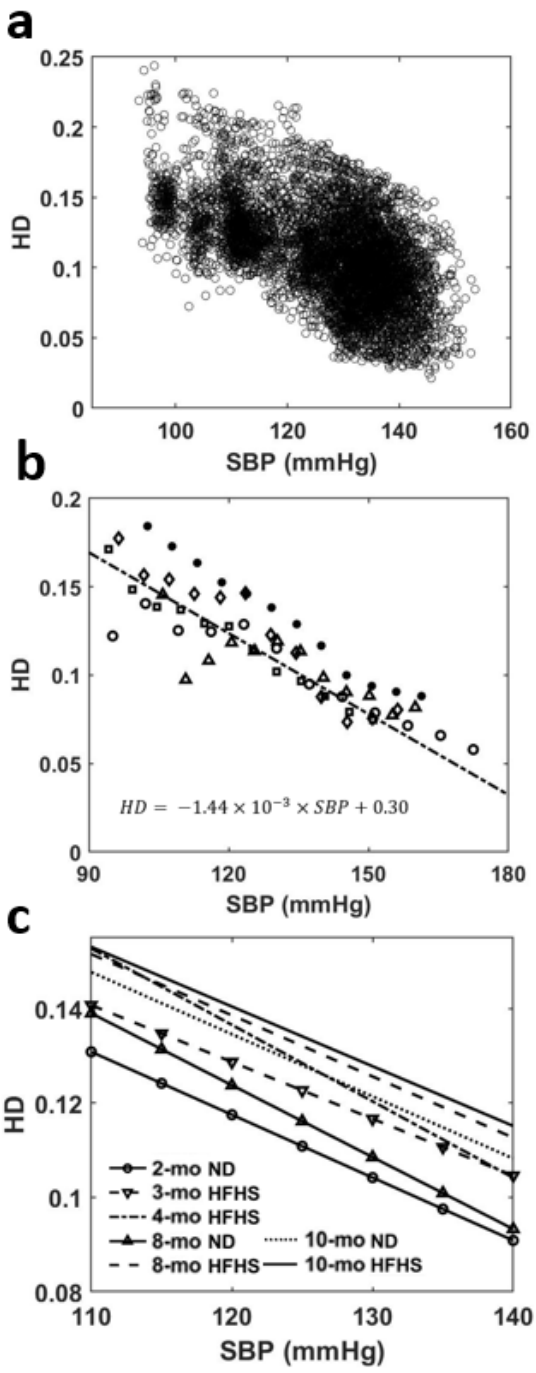

Figure 3.5: (a) HD values of individual BPW are plotted as a function of the corresponding wave's SBP. (b) Mean HD values within evenly spaced BP bins for the 8-months ND group (n = 5). Different symbols represent different mice in the group. The solid line represents a weighted linear regression ($r^2 = 0.78$) to the data from the group. (c) Linear regressions between HD and luminal SBP for the 7 age and diet groups. The linear relationships consistently trend upward with increasing age and HFHS diet.

Linear regression curves were then generated in a similar manner for all groups and plotted in Figure 3.5c. An upward vertical shift in the curves is observed with age and diet, and the shift becomes more pronounced for older mice and mice on the HFHS diet (Figure 3.5c). In the pressure range of 110–140 mmHg SBP that all mice experience, the Friedman test, which evaluated the difference between groups' HD values, reveals the relative effect of the age on ND or HFHS diet (Table 3.1). The tests paired each of the seven age and diet groups with one another, using the rising SBP readings as repeated measures and the corresponding HD values as dependent variables. Many of these pairings were found to be highly significant with $p < 0.001$, suggesting a significant difference in HD between the age and diet groups. However, no significant difference was found the between 2-months ND and 3-months HFHS ($p = 0.375$), 8-months ND and 4-months HFHS ($p = 0.977$), 8-months HFHS and 10-months HFHS ($p = 0.549$), and the two 10-months groups ($p = 0.346$).

Table 3.1: The p-values were obtained from Friedman test and Skillings-Mack test between grops. 2-months ND (n = 6), 3-months HFHS (n = 6), all other groups (n = 5). Tests were performed on average HD values with SBP bins ranging from 110–140 mmHg between each age/diet group.

	3-mo HFHS	4-mo HFHS	8-mo ND	8-mo HFHS	10-mo ND	10-mo HFHS
2-mo ND	0.375	<0.001	<0.001	<0.001	<0.001	<0.001
3-mo HFHS		<0.001	<0.001	<0.001	<0.001	<0.001
4-mo HFHS			0.977	0.002	0.007	0.002
8-mo ND				<0.001	0.008	0.002
8-mo HFHS					<0.001	0.549
10-mo ND						0.346

3.4.3 HD vs. arterial stiffness

To study the relationship between HD and arterial stiffness, we obtained tangent modulus measurements by first using the inflation test of carotid artery samples to obtain pressure radius curves (Figure 3.6a), from which the circumferential stress-stretch relationships can be calculated (Figure 3.6b). At transmural pressures between 0–60 mmHg, the tangent modulus is nearly the same for each mouse, regardless of age and diet. As pressure reaches about 60–70 mmHg, the tangent modulus increases prominently with pressure. Mice from the 10-months group were found to have a decrease in tangent modulus when compared with the 4-months group, which was accompanied by compromised energy storage capability and lower wall stress, as shown previously from others and our recent work (Gkousioudi et al., 2022). Mice on the HFHS diet appear to have lower tangent modulus values in the 4-months group, however this trend disappears in the 10-months group.

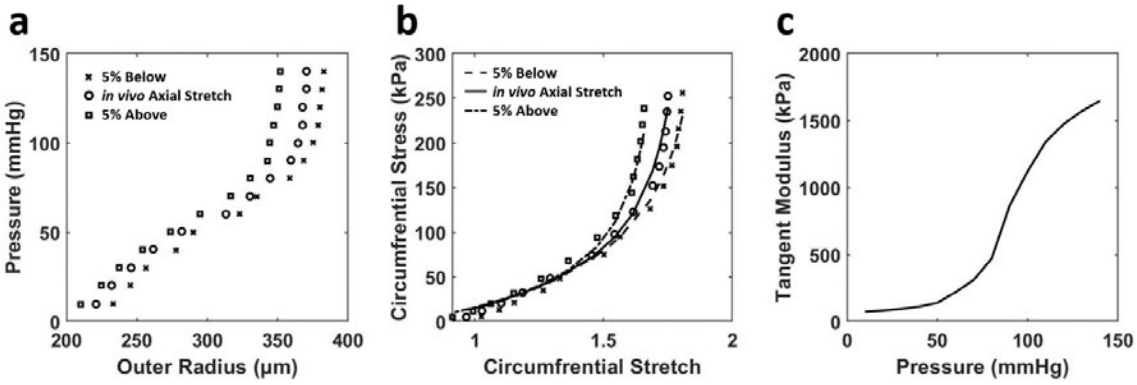

Figure 3.6: Representative results of (a) in vitro pressure-outer radius curves from biaxial extension-inflation test; (b) circumferential stress-stretch curves; and (c) tangent modulus vs. pressure of a carotid artery sample of a 4-months ND mouse with model parameter c = 20.540 kPa, $c^1{}_1$ = 3.742 kPa; $c^1{}_2$ = 0.030; $c^2{}_1$ = 11.267 kPa; $c^2{}_2$ = 0.043; $c^{3,4}{}_1$ = 0.008 kPa; $c^{3,4}{}_2$ = 1.373 kPa, and α = 46.352° (Gkousioudi et al., 2022).

For each mouse the HD value and tangent modulus at the same transmural pressure were plotted for the 4- and 10-months groups (Figures 3.7a,b) and fitted with a linear line. The average slopes of these linear fits are displayed in Figure 3.7c. Our results demonstrate there is a linear relationship between HD and tangent modulus obtained from in vitro biomechanical testing. This relationship is consistent within all mice (n = 10) from both ND and HFHS groups. Furthermore, the linear trend appears to be steeper with HFHS diet. Average perivascular pressure was used in this study; however, it is not known whether perivascular pressure changes with aging and the development of metabolic syndrome. Adopting perivascular pressures at 13.22 ± 5 mmHg had an unnoticeable effect on the linear regressions between tangent modulus and HD, although the effect of perivascular pressure on the slope of the linear regression needs to be further investigated.

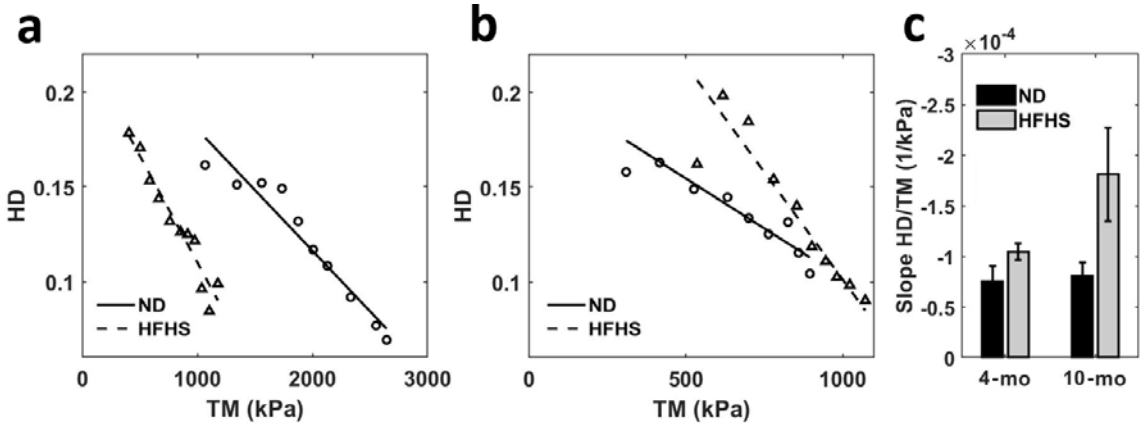

Figure 3.7: Harmonic distortion from in vivo spectral analysis as function of tangent modulus measured by in vitro biomechanical testing for the 4-months (a) and 10-months mice (b), normal (circles and solid line) and HFHS diet (triangles and dashed line). Linear regressions from each group are also displayed. (c) Average slopes of the harmonic distortion vs. tangent modulus linear fitting for the age and diet groups.

The relationship between HD and PWV, a measure of arterial stiffness in vivo, was examined by plotting the mean HD values at 115, 135, and 155 mmHg against the average PWV values for each age and diet group (Figure 3.8). The slopes of the linear fits change at different pressures as well as the slope of the two diet groups. HD increases linearly with PWV for both the control ND group and the HFHS diet group with R^2 values between 0.375 and 0.998. The slopes of the linear relationship for the ND group increase with pressure with slopes being 0.015, 0.026, and 0.040 at 115, 135, and 155 mmHg, respectively. However, the plots for the HFHS groups decrease slightly with slopes being 0.015, 0.011, and 0.008 at 115, 135, and 155 mmHg, respectively.

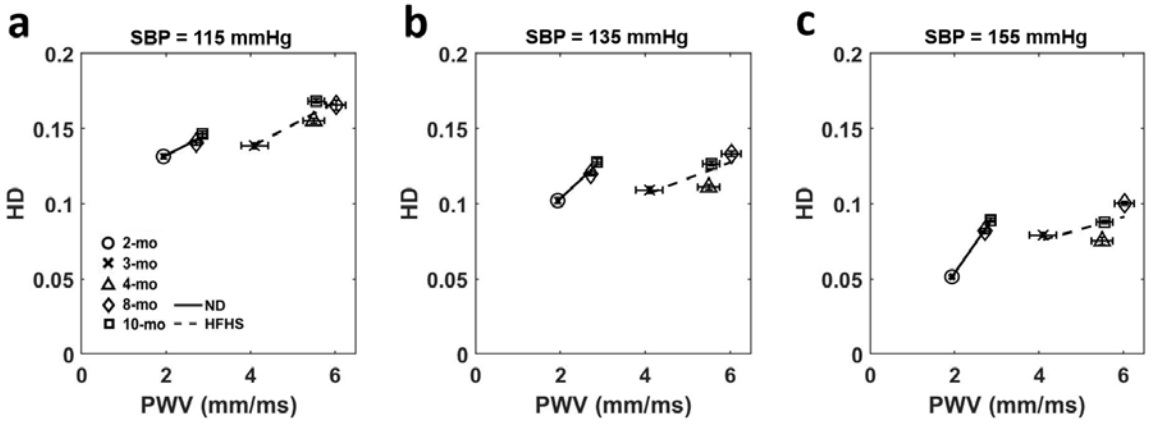

Figure 3.8: Average HD at 115 mmHg (a), 135 mmHg (b), and 155 mmHg (c) is plotted as a function of the group's corresponding average PWV, collected via Doppler ultrasound, for each age and diet group.

3.5 Discussion

BPW contains information on the coupled interactions among the forward propagating wave, reflected wave, as well as the arterial wall mechanics (Hirata et al., 2006; Ageenkova and Purygina, 2011; van Varik et al., 2012; Theodor et al., 2014). In

this study a novel index, HD, was derived from the BPW that was measured in vivo using radio telemetry in mice. The nonlinear nature of the wall mechanics combined with the reflected wave alter the BPW by changing the time delay between the forward traveling and reflected waves (Amin et al., 2012) as well as the magnitude of these waves (Ageenkova and Purygina, 2011; Theodor et al., 2014). We hypothesized that HD would be sensitive to such changes. To test this, we studied the relationship between HD and other arterial stiffness measures obtained both in vitro and in vivo. Our results suggested that HD shows promise in assessing arterial stiffness as demonstrated by the linear correlation between HD and tangent modulus, an in vitro measure of arterial stiffness, as well as with PWV, an in vivo index of arterial stiffness. Furthermore, the slopes of the relationships show dependence on diet.

Both SBP and HD show variability within individual subjects. The BPW has beat-to-beat variability with SBP varying considerably based on many factors including: PWV, age, 24-h activity level, as well as brain and nerve function (Schillaci et al., 2012; Miao and Su, 2002; Stauss et al., 2008; Yoshimoto et al., 2011). From our results over the course of 24 h, SBP also varies largely with relative day-and-night activity cycles (Figure 3.4a). The distributions of SBP followed a bimodal Gaussian form, containing a low mean and high mean SBP in mice fed ND and HFHS diet (Figure 3.4), which likely corresponds with the day-and-night cycle in which subjects experience variable blood pressures related to their relative activity levels (Vliet et al., 2003; Van Vliet et al., 2006). The SBP distributions (Figure 3.4) indicate that diet-induced metabolic syndrome

promotes a greater probability of high SBP. We have noted a significant increase in the low-pressure mode after just 1 month of HFHS diet ($p = 0.0303$). This suggests that the SBP distribution may contain an earlier manifestation of hypertension than mean BP, as used in a previous study (Weisbrod et al., 2013). High blood pressure is highly associated with increased risk of cardiovascular diseases (Kannel, 2000). Therefore, analysis of BP distribution and variability may provide insight on the physiological changes in cardiovascular function. Despite the variability in SBP and HD, our study shows that HD is linearly related to blood pressure; as SBP increases the corresponding isolated wave's HD decreases (Figure 3.5a). The trend is measurable and consistent within each age and diet group (Figure 3.5c). Elevated blood pressure is a key measure of hypertension and cardiovascular risk, though such elevation is only observed at longer time scales, in the order of months. From our study, it is important to note that beat-to-beat variability exists in SBP and BPWs. Due to the relative activity level, the mice experience high SBP in the young groups (Figure 3.4a) as well as low SBP in the old group.

The relationship between HD vs. SBP was established based on the beat-to-beat variability using 20's BPW data. Such short-term fluctuations in SBP and BPW (Figure 3.4a and Figure 3.5a) and their relationships (Figure 3.5c) have demonstrated to be different between the age and diet groups. Additionally, a key finding of our study is that HD is strongly associated with arterial wall stiffness, an independent cardiovascular risk factor that cannot be derived from SBP alone.

HD analysis of the BPW indicates that the BPW undergoes changes with age and diet-induced metabolic syndrome, both of which are linked to changes in arterial wall stiffness (Blacher et al., 1999; Nichols, 2005; Wilkinson et al., 2002b; Brooks et al., 2001; Brooks et al., 1999; Wilkinson et al., 2000). The inverse linear relationship between HD and SBP (Figure 3.5b) suggests that HD is sensitive to changes in arterial stiffness, since with higher mean blood pressure, arterial stiffness increases (Figure 3.6c). This is further confirmed by the inverse linear relationship between HD and the tangent modulus (Figures 3.7a and Figure 3.7b). At higher blood pressures, there is an increase in arterial stiffness due to the gradual recruitment of collagen fibers in the adventitia (Chow et al., 2014), which would impact the BPW and thus HD. Moreover, with arterial stiffening, the waveform peak is augmented due to the overlapping of the forward and reflected waves (van Varik et al., 2012), leading to higher distortion of the BPW (Figure 3.5c). This overlap is largely originated from increased speed of both wavelets, coupled with earlier reflections during arterial remodeling (van Varik et al., 2012). Spectral decomposition of stress waveforms via a Fourier transform has been used in a previous study to characterize mechanical nonlinearity of isolated rat aorta (Imsirovic et al., 2018). Future study is required to understand the role of nonlinear arterial wall properties in relation to HD. The relationship between HD and arterial stiffness is liable to shift with age and, more significantly, diet. There is also an apparent increase in slope of this relation for each age and diet group (Figure 3.7c). Consistent with previous findings that hypertension develops after 6 months of HFHS diet (Weisbrod et al., 2013), the 8-months HFHS group has significantly higher HD values than the 8-months ND group ($p < 0.001$)

(Table 3.1). Further, the two 10-months groups (both ND and HFHS) are not different with regards to their HD trends, which implies that changes due to diet have slowed or subsided by 10-months. Nonetheless, the two old ND groups (8-months and 10-months) contain significantly different HD values ($p = 0.008$) suggesting change in HD still occurs in ND aging after the mice have reached maturity. In contrast, the 8-months HFHS group's HD values are not significantly different from 10-months HFHS ($p = 0.549$). This supports the idea that changes in the arterial wall mechanics have already occurred in the 8-months HFHS group. The efficacy of detecting this change supports HD as a noninvasive predictor of hypertension which warrants further studies.

PWV is a broadly used in vivo index of arterial stiffness that measures the velocity of the forward propagating arterial pressure wave (Blacher et al., 1999; Nichols, 2005). When studying the relationship between HD and PWV (Figure 3.8), it is important to note that HD, derived from beat-to-beat BPW, is pressure dependent while PWV is not. We found that HD and PWV to be linearly related but with a diminishing R squared value in the HFHS group related to increasing pressure (Figure 3.8). Further study is needed to better understand the pressure and diet dependency of this relationship. The positive HD-PWV relation is in contrast to that of the tangent modulus and HD, which demonstrated a negative relation (Figure 3.7). While the explanation for this is not entirely clear, these results suggest that the tangent modulus is also negatively related to PWV. Possible explanations include the following. The PWV measurements were made in the abdominal aorta while HD was obtained from BPWs at the aortic arch. Abdominal

aorta has been reported to be more severely affected by vascular remodeling (Hayashi et al., 2010), which could account for the more dramatic change seen in PWV with age and diet as compared to HD (Figure 3.8). Notably, the ND and HFHS diet groups follow their own linear paths (Figure 3.6c). It is also important to point out that HD is derived from local BP measurement, taken in a point within the aortic arch where the radiotelemetry is surgically implanted within the mouse, while PWV is usually obtained over a segment length of ~1 cm. This suggests that HD can potentially be used to reveal the regional dependent condition of the arterial wall, independently of PWV.

When considering HD, it is important to mention arterial impedance as both HD and impedance rely on Fourier transforms of the BPWs (Kelly and Fitchett, 1992). Impedance is calculated by the ratio of Fourier amplitudes from the BPW and velocity waveforms, which provides an impedance modulus and phase over a range of frequencies (Kelly and Fitchett, 1992), and the modulus has been shown to increase with age-related arterial stiffening (Reddy et al., 2003). However, impedance analysis requires invasive methods and it does not consider the effect of BP on Fourier coefficients from BPWs. Previous studies on input impedance have shown inconsistencies when relating impedance directly to PWV after adjusting for factors like mean blood pressure (Mitchell et al., 2002; Segers et al., 2007b). Our results of the HD dependence on SBP (Figure 3.5a) suggest that HD, or the Fourier coefficients, of BPWs change with SBP and such changes should be considered when studying BPW.

3.6 Limitations

Our study has several limitations. Future studies including the 3- and 4-months ND groups may be necessary for direct comparison with the 3- and 4-months HFHS groups, although our previous study showed that the 2-, 3-, and 4-months ND groups do not show significant differences in arterial stiffness and blood pressure measures (Weisbrod et al., 2013). Only male mice were used in this study. Dependence of BPW and HD index on sex also warrants further studies. Additionally, the number of mice should be increased to make quantitative comparisons between HD and tangent modulus among different age and diet groups. The radiotelemetry BPW readings were taken in the aortic arch at the left carotid artery. Due to the proximity of aortic arch and carotid arteries, it was assumed that pressure taken at the arch would be an acceptable estimation of pressure within the carotid artery in order to compare HD derived from BPWs with tangent modulus from direct in vitro stiffness. This study uses surgically implanted telemetry for BPW, but other more accessible approaches such as BP tonometry could produce the waveforms required for this analysis (Parry Fung et al., 2004; Feng and DiPetrillo, 2009). PWV was measured over the abdominal aorta. Differences between the material properties and the progression of arterial stiffening varies between arteries (Hayashi et al., 2010) and therefore regional variation in mechanical properties of arteries should be kept in mind while making comparisons. The interference between radiotelemetry and BPW is not known. The HD index cannot differentiate between reflection and local wall properties. Clinical studies are needed to dissect the contribution of individual factors, such as hemodynamics and wall properties, to BPW and HD.

3.7 Summary

BPW contains a wealth of information from the interactions of the forward and backward propagating waves, arterial wall mechanics, and hemodynamics. In this study, HD is proposed as a novel index to assess changes in arterial mechanical function. We showed that HD, obtained based on Fourier transform of individual BPWs, is related to SBP, and other existing in vitro and in vivo arterial stiffness measures. HD is also sensitive to age and metabolic syndrome-induced changes in BPW. Instruments used to record BPWs are more readily available clinically than instruments used to record flow. Hence, our results demonstrate that HD has the potential to be used as a noninvasive and easily accessible means.

CHAPTER 4 BLOOD PRESSURE WAVEFORM MORPHOLOGY ASSESSED USING TRANSMISSION LINE MODEL AND HARMONIC DISTORTION ANALYSIS

4.1 Overview

Blood pressure waveform (BPW) is an easily accessible measure of changing blood pressure over a short period of time. A major determinant of BPW morphology is vascular impedance, governed by the material properties of the arterial wall and the hemodynamics of blood flow. Analysis of BPW morphology can be an effective means of assessing cardiovascular health. We implemented a transmission line model of the mechanical impedance of the arterial tree that can recreate physiologically realistic BPWs. We then examined the sensitivity of existing vascular measures, including augmentation index (AI), pulse wave velocity (PWV), and the recently proposed harmonic distortion (HD), to structural and mechanical parameters of vessel walls and blood flow. All three measures are primarily sensitive to structural stiffness while HD and AI also correlate strongly with geometric parameters. Further, in a simulated clinical study of randomly constructed arterial trees using model parameters within a physiological range, the indexes are strongly correlated with stiffness. When controlling for all confounding factors, HD demonstrates a stronger correlation with arterial stiffness than AI for stiffness values higher than the average. Overall, using a transmission line model, our study provides a mechanistic understanding of the determinants of AI and HD, with the latter being a promising measure of cardiovascular risk due to its ease of

calculation and access, meeting key limitations set by AI and PWV.

4.2 Introduction

Aortic stiffening, as a consequence of adverse remodeling and breakdown of elastic fibers, is associated with higher risk for cardiovascular disease and other chronic diseases of ageing (Van Varik et al., 2012; O'Rourke et al., 2016; Ferruzzi et al., 2018a). Therefore, there is growing interest in techniques that can be used to assess arterial stiffness in the clinic. One approach is to assess changes in morphology of the blood pressure waveform (BPW), a recording of blood pressure as a function of time. The features of a BPW manifest from the blood flow interacting with various sources of mechanical impedance such as wall stiffness throughout the vasculature (Mitchell, 2008; Westerhof and Westerhof, 2018; Westerhof et al., 2020). Certain features of BPW, such as wave reflection present in the aggregate waveform, increase with age through midlife and may be associated with cardiovascular risk (Mitchell et al., 2004). However, previous studies have yielded mixed relations of wave reflection measures with cardiovascular risk, which has limited further investigation (Hirata et al., 2006; Mitchell, 2008; Jerrard-Dunne et al., 2008; Ageenkova et al., 2011). Although previous attempts have focused on pressure differentials between waveform features (Mitchell et al., 2004; Jerrard-Dunne et al., 2008; Ayer et al., 2010; Ageenkova et al., 2011), this method proved inconsistent due to the different BPW morphologies corresponding to aging and cardiovascular conditions (Chen et al., 1996).

The BPW is made up of two dominant waves: a forward wave generated from the heart and an aggregate or global reflected wave produced by differences in characteristic impedances between contiguous vessels (Burattini et al., 1991; Wilkinson et al., 2002b; Hirata et al., 2006; Mitchell, 2008). The reflected wave augments the forward wave to produce a characteristic shoulder in BPW, which is used to quantify wave reflections via the augmentation index (AI), which measures changes in BPW morphology solely from peak pressure differences between the two waves (Wilkinson et al., 2002b; Ayer et al., 2010). Wave reflection in general is known to play a role in cardiovascular risk, though how wave reflection relates to arterial heath is still not fully understood (Wilkinson et al., 2002b; Hirata et al., 2006; Mitchell, 2008; Ageenkova et al., 2011). Past studies have attempted to connect AI to pulse wave velocity (PWV), a gold-standard index of arterial stiffness, calculated using the difference in arrival times of pressure waveforms over a measured length of artery (Blacher et al., 1999; Nichols, 2005). These studies have shown that AI increases linearly with PWV, except for individuals 60 and older where AI was shown to decrease (Mitchell et al., 2004)**Error! Reference source not found.**. The resulting nonlinear relations of AI with aortic stiffness suggest that wave reflections may be affected by more complex interactions between hemodynamics and vessel biomechanics, which are known to change with age (Mitchell et al., 2004; Sun, 2015). The limitations of AI as an index have impeded its relevance in recent years, favoring the more reliable PWV, which does not require waveform shape information (Hirata et al., 2006). Nevertheless, published measurements of PWV commonly require specialized equipment and training, which may not be available in all clinics. Recently, we introduced an index,

harmonic distortion (HD), (Milkovich et al., 2022) a frequency-domain assessment of BPW morphology that is an easily accessible measure of the arterial pressure response to blood flow. Using a mouse model, we showed that HD is correlated with stiffness of carotid artery, from both *in vivo* and *in vitro* measurements, and with age, suggesting that HD is sensitive to arterial stiffening.

Transmission line models have been used to study effects of wall properties on BPWs when the vasculature is modeled as a network of mechanical impedances (Noordergraaf et al., 1963; Westerhof et al., 1969; Avolio, 1980; Stergiopulos et al., 1992; Ferrari et al., 2000; Davies et al., 2012; Masuda et al., 2013). These models utilize electrical components to approximate impedance to blood flow, an approach that was first conceptualized in the late 1950s (Womersley, 1957). Some of the first transmission line models were then developed and validated, with the application of the model in the human arterial tree published in 1969 (Westerhof et al., 1969). The model was then implemented to study arterial stenosis (Avolio, 1980; Stergiopulos et al., 1992) and showed that narrowed vessels correspond to higher PWV. Stergiopulos et al., 1992 studied Windkessel values and the effect of different terminating complex impedances on blood flow, varying the number and configuration of elements which importantly defines the 3-element standard. Davies et al., 2012 further showed that wave reflections originate from multiple smaller reflection sites rather than one large discrete site, which is important for understanding the nature of wave propagation within the complex arterial system. Westerhof et al., 2020 has recently published results from a 121-segment model

in combination with a detailed aging model to recreate increasing aortic PWV with age.

The primary goal of this study was to establish the biomechanical contributors to our recently introduced index, HD. To this end, we implemented a transmission line model and compared HD to other existing arterial function measures, AI and PWV, under a variety of simulated physiological and pathological conditions. Specifically, the model was used to simulate a physiological BPW, from which HD, AI, and PWV were calculated. Using, sensitivity analysis, the effects of various biomechanical parameters of the arterial wall and blood flow on BPW and associated indexes were studied. Furthermore, the model was also used to simulate a clinical scenario by generating arterial trees with biomechanical and geometrical parameters systematically varied to represent a population of subjects to help better understand the relative contribution of these variables to HD, AI and PWV.

4.3 Material and methods

4.3.1 Transmission line model

A transmission line model was implemented that consists of the aorta and its subtended tree-segments as detailed by Westerhof et al., 2020 (Table 4.1) and shown in Figure 4.1. The ends of the transmission line are terminated with a complex impedance described by the three-element Windkessel model (Figure 4.2a) (Stergiopulos et al., 1999) using values reported by Stergiopulos et al[Error! Reference source not found.]., 1992 (Table

4.2) which account for the impedance generated by further distal branches. The model consists of 36 segments (Westerhof et al., 2020), representing the arterial tree of an adult male, with vessel name and data listed in Table 4.2. In our model, there are 25 distal terminations that need to be defined. According to Westerhof et al., 2020, these distal segments were terminated with three-element Windkessel models that consists of a downstream parallel peripheral resistance and capacitance, and an upstream resistance. The aggregated properties of these Windkessel models represent the effects of smaller branch vessels not included in the main arterial tree. We implemented the transmission line model in MATLAB (Natick, Massachusetts, USA) and calculated the average geometric and Young's modulus values. These averages were derived from the 121-segment Westerhof model. Specifically, we summed the lengths of the artery segments covered by our 36-segment model. Additionally, we determined the average values for the remaining parameters, which include radius and structural stiffness.

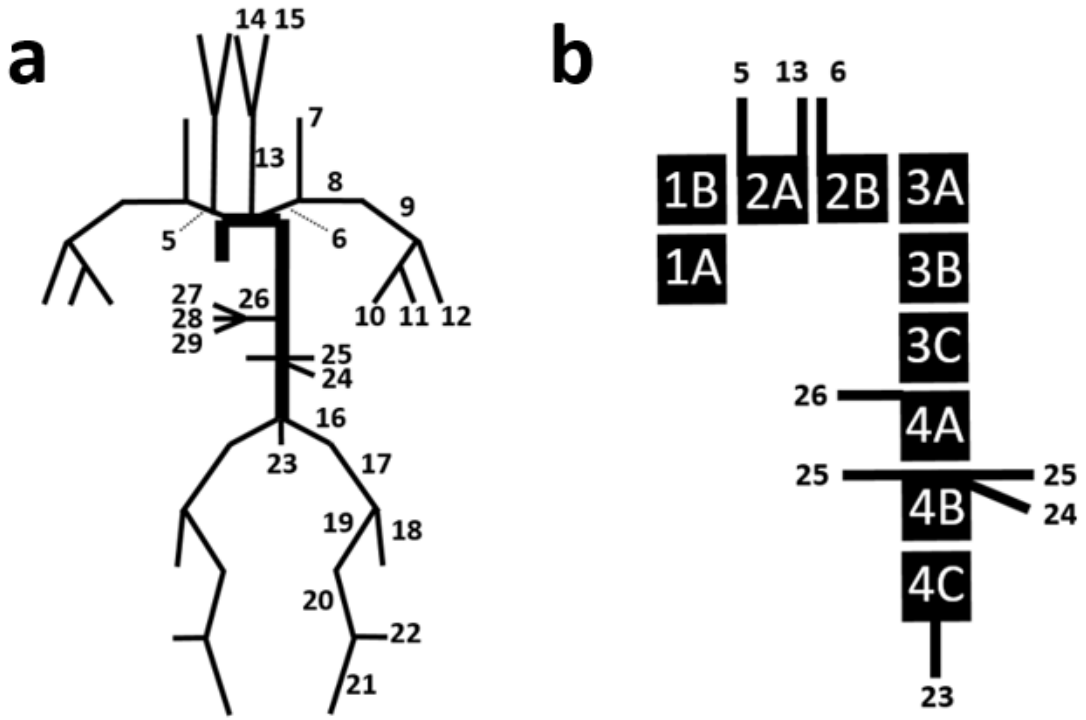

Figure 4.1: (a) Transmission Line schematic illustrating each vessel segment's location and connection to other segments, representing an adult male. Numbers correspond to vessel names and data compiled in Table 4.1. Segments not labeled are reflected duplicates from the opposite side of the system. Ends of the transmission line are terminated by the Windkessel model, see Table 4.2. (b) The aorta is broken up into sub-segments. The schematic also illustrates the locations at which the system branches into further subtrees.

Table 4.1: Anatomical data corresponding to Figure 4.1 (Westerhof et al., 1969; Westerhof et al., 2020)

	Vessel Segment	L (cm)	r (cm)	h (cm)	E (MPa)	Paired
1A	Ascending Aorta	2.00	1.47	0.16	0.40	N
1B	Ascending Aorta	2.00	1.44	0.16	0.40	N
2A	Aortic Arch	2.00	1.40	0.13	0.40	N
2B	Aortic Arch	3.90	1.20	0.13	0.40	N
3A	Thoracic Aorta	5.20	1.10	0.12	0.40	N
3B	Thoracic Aorta	5.20	1.00	0.11	0.40	N
3C	Thoracic Aorta	5.20	0.90	0.10	0.40	N
4A	Abdominal Aorta	5.30	0.80	0.09	0.40	N
4B	Abdominal Aorta	5.30	0.65	0.08	0.40	N
4C	Abdominal Aorta	5.30	0.60	0.08	0.40	N
5	Brachiocephalic	3.40	0.62	0.09	0.40	N
6	Left Subclavian	3.40	0.42	0.07	0.40	N
7	Vertebral	14.20	0.19	0.05	0.80	Y
8	Axilliary	18.50	0.36	0.06	0.40	Y
9	Brachial	23.50	0.26	0.05	0.40	Y
10	Ulnar	23.80	0.16	0.05	0.80	Y
11	Interossea	7.90	0.09	0.03	1.60	Y
12	Radial	23.50	0.16	0.04	0.80	Y
13	Common Carotid	20.80	0.37	0.06	0.40	Y
14	Internal Carotid	17.70	0.13	0.04	1.07	Y
15	External Carotid	17.70	0.13	0.04	1.07	Y
16	Common Iliac	5.80	0.34	0.07	0.40	Y
17	External Iliac	8.30	0.31	0.06	0.40	Y
18	Profundis	12.60	0.19	0.05	1.60	Y
19	Femoral	31.50	0.25	0.05	0.40	Y
20	Popliteal	18.90	0.20	0.05	0.80	Y
21	Posterior Tibial	32.10	0.14	0.05	1.60	Y
22	Anterior Tibial	34.30	0.14	0.04	1.60	Y
23	Inferior Mesenteric	5.00	0.16	0.04	0.40	N
24	Superior Mesenteric	5.90	0.20	0.07	0.40	N
25	Renal	3.20	0.26	0.05	0.40	Y
26	Coeliac	1.00	0.39	0.06	0.40	N
27	Gastric	7.10	0.18	0.05	0.40	N
28	Splenic	6.30	0.28	0.05	0.40	N
29	Hepatic	6.60	0.22	0.05	0.40	N

Table 4.2: Windkessel values corresponding to Figure 4.1 and Figure 4.2a (Stergiopulos et al., 1992; Westerhof et al., 2020)

Vessel End	*Rs* $(N \cdot s/m^5) \cdot 10^5$	*Rp* $(N \cdot s/m^5) \cdot 10^5$	*Cp* $(m^5/N) \cdot 10^{-5}$
7	7705	25313	6.19E-06
10	20230	72750	7.05E-06
11	67107	633750	4.41E-07
12	19614	120000	7.05E-06
14	111303	120937	2.68E-06
15	111303	120937	2.68E-06
18	16140	35850	7.80E-06
21	39471	35850	7.80E-06
22	32341	42000	6.66E-06
23	10358	51750	5.41E-06
24	7250	10519	3.29E-05
25	3567	12825	3.29E-05
27	8008	60975	6.88E-06
28	3170	26213	1.60E-05
29	5168	40950	1.03E-05

Each segment of the tree, representing the blood-arterial wall interactions, is represented by a linear circuit of complex impedances composed of a series or longitudinal impedance, axial pressure gradient over flow, and a parallel or transverse impedance, pressure over axial flow gradient (Avolio, 1980; Stergiopulos et al., 1992). Figure 4.2b shows a single unit of the transmission line representation of a vessel.

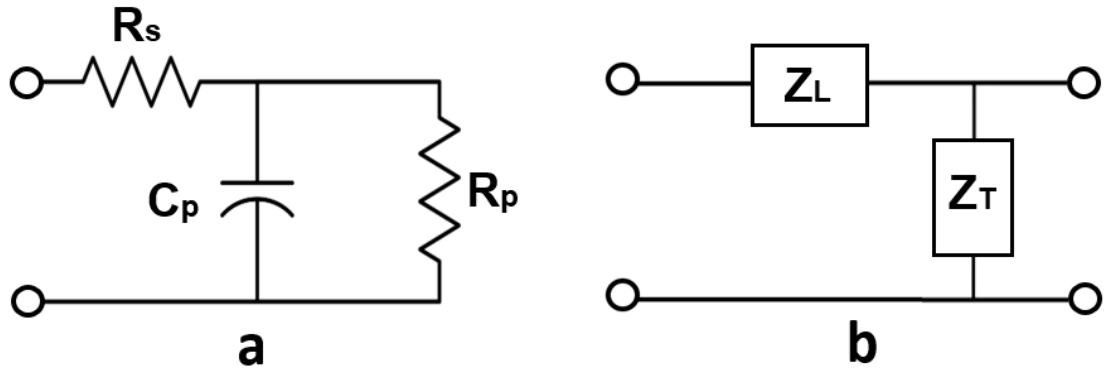

Figure 4.2: (a) Three-element Windkessel impedance model which terminates each of the ends of the arterial tree. Resistors and capacitor represent series resistance (Rs), parallel resistance (Rp), and parallel compliance (Cp). (b) Representation of a single vessel segment modeled as a circuit containing both longitudinal (ZL) and transverse impedance (ZT). Circles are drawn to represent the points of connection to the next segment in the transmission line.

The longitudinal impendence (Z_L), defined by blood properties, and the transverse impedance (Z_T) from the arterial wall properties per unit length of the vessel are defined as (Jager et al., 1965):

$$Z_L = R + i\omega L \tag{4.1}$$

$$Z_T = \frac{1}{i\omega C} + R_T \tag{4.2}$$

Where *R* and *L* are the series resistance and inductance, respectively, *C* is the parallel capacitance, and ω is the angular frequency (Figure 4.2b). The *R* corresponds to the resistance to blood flow in the vessel related to blood viscosity (μ) and governed by Poiseuille's law (Avolio, 1980; Jager et al., 1965):

$$R = \frac{8\mu}{\pi r^4} \tag{4.3}$$

where *r* is the inner radius of the vessel. A discrete approximation of flow in a cylindrical

tube provides a relationship between *L,* blood density (ρ) and *r*, while *C* is related to the modulus of the arterial wall *E* (Avolio, 1980; Jager et al., 1965);

$$L = \frac{9\rho}{4\pi r^2} \tag{4.4}$$

$$C = \frac{3\pi r^3}{2Eh} \tag{4.5}$$

where *h* is the thickness of the vessel wall and *E* is the Young's modulus of the arterial wall. The transverse impedance of the arterial wall includes both elastic and viscous components as (Taylor, 1959a; Taylor, 1959b; Westerhof and Noordergraaf, 1970):

$$R_T = \frac{2\mu_w \omega h}{3\pi r^3} \tag{4.6}$$

Here, μ_w is the wall viscosity. The viscoelastic properties of the arterial wall are determined by angle ϕ, the phase between pressure and wall displacement (Avolio, 1980):

$$\mu_w = \frac{E\tan(\phi)}{\omega} \tag{4.7}$$

Angle ϕ is usually frequency dependent and can be defied as

$$\phi = \phi_0(1 - e^{-2\omega}) \tag{4.8}$$

where ϕ_0 is a viscoelastic constant (Avolio, 1980; Westerhof and Noordergraaf, 1970). In order to account for the differences in viscoelasticity between elastic and muscular arteries, we have chosen to represent the aorta with one third the viscoelastic magnitude ϕ_0 as compared to the elastic branch vessels (Westerhof and Noordergraaf, 1970).

The characteristic impedance (Z_0), propagation coefficient (γ), and reflection coefficient (Γ) of a vessel segment are determined by the vessel's transverse and longitudinal impedances, Z_T and Z_L, as well as its load impedance (Z_{Load}) (Taylor, 1966; Van den Wijngaard et al., 2008), respectively, as the following:

$$Z_0 = \sqrt{Z_L Z_T} \tag{4.9}$$

$$\gamma = \sqrt{\frac{Z_L}{Z_T}} \tag{4.10}$$

$$\Gamma = \frac{Z_{Load} - Z_0}{Z_{Load} + Z_0} \tag{4.11}$$

where Z_{Load} is the termination impedance at the end of the transmission line of a given segment, or simply the impedance to the distal end in Figure 4.2b. Finally, the input impedance of the vessel of length *l*, can be calculated using Equations 4.9–4.11 (Van den Wijngaard et al., 2008):

$$Z_i = Z_0 \left[\frac{1 + \Gamma e^{-2\gamma l}}{1 - \Gamma e^{-2\gamma l}}\right] \tag{4.12}$$

To calculate the total input impedance of the tree, starting from the end, the input impedance of a segment becomes the load impedance as the transmission line iterates from the end of the line towards the heart (Van den Wijngaard et al., 2008). When two segments meet at a bifurcation, the impedances of the segments are added in parallel (Haidar et al., 2021). Hence, the total input impedance of the system (Z_{iT}) can be

calculated. The time domain representation of BPW can then be computed as:

$$BPW = \mathcal{F}^{-1}\{Q \times Z_{iT}\} \tag{4.13}$$

where Q is the Fourier transform of the flow waveform arriving from the heart and $\mathcal{F}^{-1}$ denote the inverse Fourier transform. A physiological aortic flow waveform was used here to generate BPWs from the model (Mitchell et al., 2003).

4.3.2 Harmonic distortion

The computed BPW is used to derive HD and AI. The properties of the arterial model are used to compute aortic PWV. HD is determined using BPW analysis in the frequency domain (Milkovich et al., 2022), as Equation 2.3 where $|A_k|^2$ are the spectral coefficients of a single BPW in the frequency domain multiplied by their complex conjugates. Thus, HD is essentially the ratio of energy above the fundamental frequency to that at the fundamental frequency of the waveform (Milkovich et al., 2022). Fourier coefficients higher than the 20th were found to be negligible since they did not significantly contribute to the HD value. For an ideal sinusoidal wave, the HD value is 0. Changes to our model which manifest as changes in BPW shape should be reflected in HD.

4.3.3 Augmentation index

As previously discussed, AI is another index that measures relative wave reflections (Ayer et al., 2010). It is defined by Equation 2.2 and Figure 1.1, where *PP* is the pulse pressure, evaluated as the difference between systolic peak and diastolic trough,

and *AP* is augmentation pressure, which is the difference in pressure between the peak of the aggregate waveform and the systolic inflection point that represents return of the reflected wave to the central aorta (Figure 1.2). To locate this inflection point, the time point was determined at which the second derivative of the waveform equals zero.

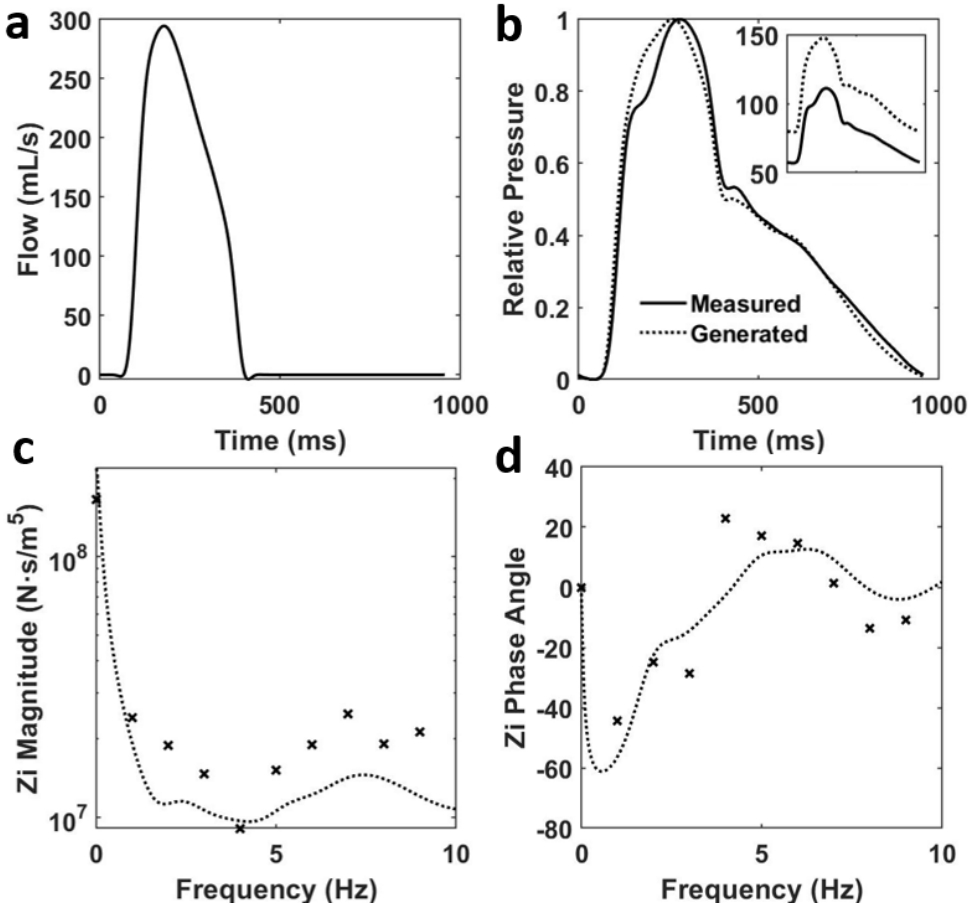

Figure 4.3: (a) An adult aortic flow waveform measured over 0.98 seconds (Mitchell et al., 2003). (b) The corresponding BPW (Mitchell et al., 2003) is plotted along with a generated BPW from the transmission line model on a relative pressure scale. The subplot shows the true pressures, in mmHg, and pulse pressures of the waveforms. The corresponding input (c) impedance magnitude and (d) phase are plotted with the generated impedance from the transmission line model and the measured value from Mitchell et al., 2003 represented by dotted lines and symbols, respectively.

4.3.4 Pulse wave velocity

Our model also allows the calculation of PWV using the arterial path from carotid to femoral arteries, which is commonly used in clinical setting for the calculation of PWV (Blacher et al., 1999; Nichols, 2005; Mitchell, 2009). First, phase velocity in a single segment is calculated as:

$$c = \frac{\omega}{imag(\gamma)} \tag{4.14}$$

Then the time that BPW spends in each segment along the carotid-femoral path is calculated as:

$$t = \frac{l}{c} \tag{4.15}$$

Next, PWV across the carotid-femoral path is calculated as the ratio of the sum of the segment lengths and the sum of the corresponding times. The carotid time and distance was subtracted from the parallel aortic time and distance (Mitchell et al., 2002).

4.3.5 Sensitivity analysis

From Equations 4.3–4.5 and 4.12, we have identified six parameters and determined their influence on BPW: 4 vessel parameters (*Eh, ϕ_0, l, r*) and 2 blood parameters (ρ and μ) (Table 4.3). *Eh* represents Young's modulus x wall thickness, which is referred to as structural stiffness (Humprey et al., 2016). In order to assess the effects of these parameters on BPW morphology and indexes, using the parameter values reported by Westerhof et al., 1969 and Stergiopulos et al., 1992 as baseline values, we varied each

individual parameter between 25% and 175% of the baseline value, while all other parameters were held constant. The BPWs produced were plotted in order to assess qualitative changes in key waveform features. The corresponding HD, AI, and PWV were also recorded, and the percent change from the baseline index was plotted.

4.3.6 Randomly generated arterial trees

Table 4.3: Physiological ranges of vessel and blood parameters in ascending aorta.

Variable	Unit	Baseline	Min	Max	Source
Modulus x Thickness, *Eh*	*N/m*	656	225	2500	(Guala et al., 2019)
Viscoelastic Phase, ϕ_0	°	15*	10	20	(Taylor, 1959b; Westerhof & Noordergraaf, 1970)
Length, *l*	*mm*	40	40	100	(Sugawara et al., 2008)
Radius, *r*	*mm*	14.55	12.5	20	(Redheuil et al., 2011)
Blood Viscosity, μ	*cP*	3.5	3	11	(Lowe et al., 1980)
Blood Density, ρ	kg/m^3	1060	990	1100	(Kenner, 1989)

* The aorta has a baseline viscoelastic phase of 5°

In an effort to mimic cardiovascular variabilities within a clinical group, arterial trees (N = 1000) were uniformly distributed using parameters of artery dimensions, and the wall and blood properties in the physiological range, see Table 4.3 for ascending aorta (Table 4.3). HD, AI and PWV were determined for every generated BPW. To eliminate BPWs with combinations of parameter values that may not be physiologically possible, we incorporated minimum and maximum bounds based on the published data from Mitchell et al., 2010a. The foregoing study examined adults between 19 and 90 years of age, with AI and carotid-femoral PWV recorded for each 10- year age group (Mitchell et al., 2010a). By plotting AI and PWV data points for male participants, we created a permissible range of AI values given a measured PWV value within a 95% confidence

interval (Mitchell et al., 2010a). This filter allowed us to filter BPWs representing an arterial tree which would produce index values beyond the physiologically observed range.

4.3.7 Statistical analysis

For the 1000 randomly generated arterial trees, partial correlation tests were performed that assessed the three indexes (HD, AI and PWV) against *Eh* while controlling for all other confounding factors. $p < 0.05$ is considered to be statistically significant.

4.4 Results

4.4.1 Efficacy of the transmission line

An aortic flow waveform was randomly selected from a normotensive group of adults used in a previous study of hypertensive versus normotensive groups (Mitchell et al., 2003). This waveform (Figure 4.3a) was used in combination with the parameters of the Westerhof et al., 2020 transmission line model to produce BPWs (Figure 4.3b). The corresponding input impedances are also plotted to illustrate that the modeled arterial tree produced impendence spectra that are comparable to those of a real human vascular tree in both magnitude and phase (Figure 4.3c and Figure 4.3d). The first important characteristic feature to note is the large impedance magnitude at zero frequency representing the total fluid flow resistance of the transmission line. The impedance

magnitude then decreases rapidly with increasing frequency due to the decreasing magnitude of Z_T. The key feature of the impedance phase is an initial sharp dip followed by a rise and oscillations around zero.

4.4.2 Parameter sensitivity

The baseline arterial tree was modified for each independent parameter from 25% to 175% as described in the Methods. The three geometric parameters resulted in the most significant changes to BPW shape (Figure 4.4). The remaining three parameters, viscoelastic phase as defined by Equation 4.8, blood density and blood viscosity, did not show a percent change in any of our cardiovascular indexes (HD, AI, PWV) greater than 20% (Figure 4.5). The exception being blood density, the value of which does not vary as widely as the sensitivity analysis assessed (Table 4.3). It is for these reasons that these parameters were deemed as negligible to the changes in cardiovascular index (Figure 4.5).

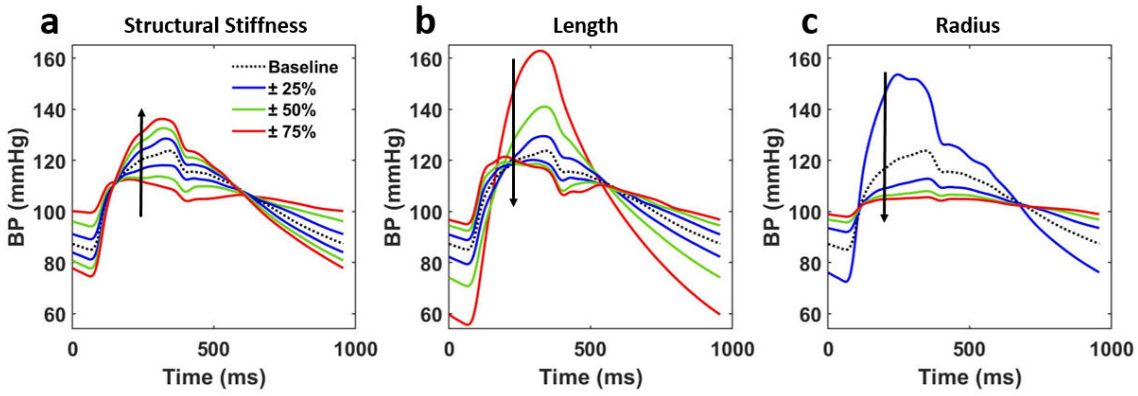

Figure 4.4: Morphology evolution of the BPW when controlling for all vessel and blood parameters but one: (a) structural stiffness, (b) length, (c) radius. Parameters of interest are incrementally scaled between 25% and 175% of the baseline value. Arrows show the direction of increasing the parameters.

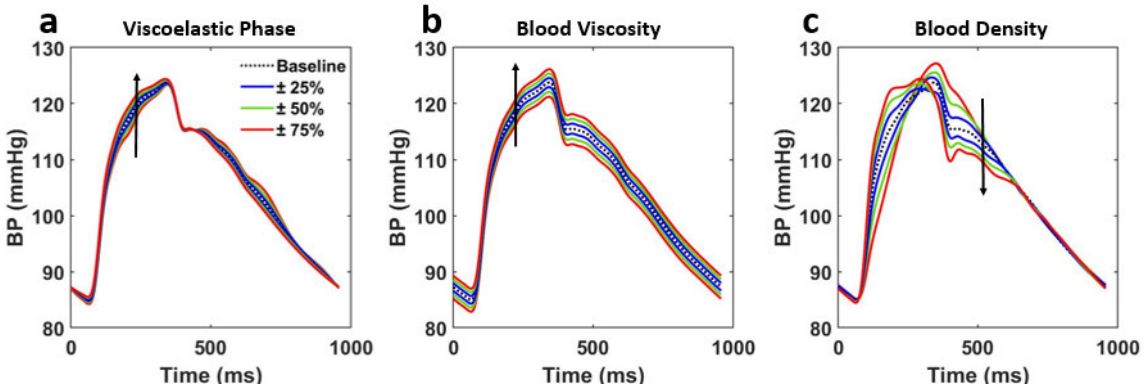

Figure 4.5: Morphology evolution of the BPW when controlling for all vessel and blood parameters but one: (a) wall viscoelasticity, (b) blood viscosity, (c) blood density. Parameters of interest are incrementally scaled between their physiological minimum and maximum, represented by α

The BPWs change in shape when model parameters are modified from their baseline values. However, each parameter has a differing effect on both the magnitude of change as well as the waveform features in question. For example, increasing vessel radius has the largest effect on blood pressure magnitudes while compared to increasing

structural stiffness. We can also observe changing reflected wave time with respect to the forward wave, most prominently in increasing vessel length which results in earlier reflected peak arrivals.

At each of the seven values for the parameters shown in Figure 4.4, cardiovascular indexes were also recorded and plotted (Figure 4.6). The greatest percent change in these indexes from the baseline was observed when the geometric parameters were varied. These three parameters change by an order of approximately 400% from the baseline value and opposite ends for their ranges which demonstrates a strong sensitivity for both HD and AI calculations. HD experiences the greatest change from the baseline by modulating structural stiffness, while AI experiences the greatest change by vessel radius. PWV, by comparison to the other two indexes, is significantly less sensitive to all three parameters.

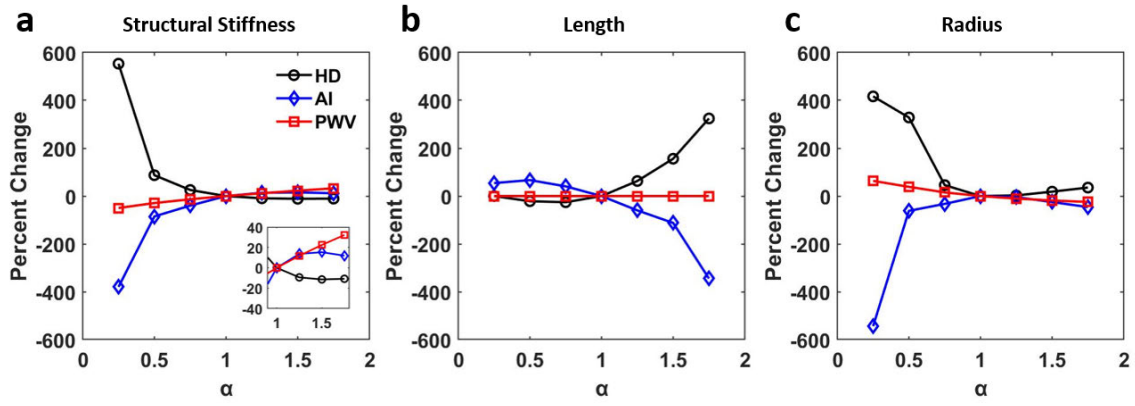

Figure 4.6: Index evolution corresponding to the changes made in Figure 4.4. (a) structural stiffness, (c) length, (d) radius.

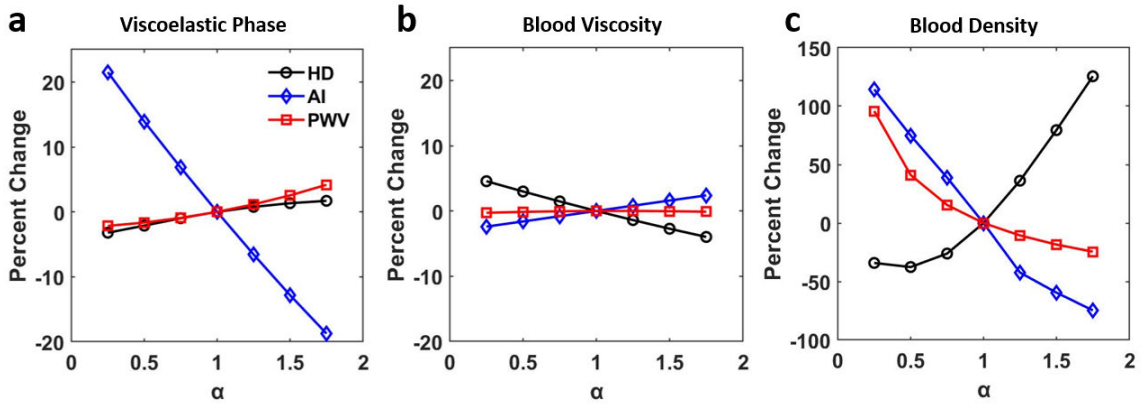

Figure 4.7: Index evolution corresponding to the changes made in Figure 4.5. (a) viscoelastic phase, (b) blood viscosity, (c) blood density

4.4.3 Random tree generation

Random values within the physiological ranges were assigned to the six vessel and blood parameters and the resulting index values computed from the corresponding BPWs are plotted (Figure 4.8). We observed a strong relationship to varied vessel length for both HD and AI.

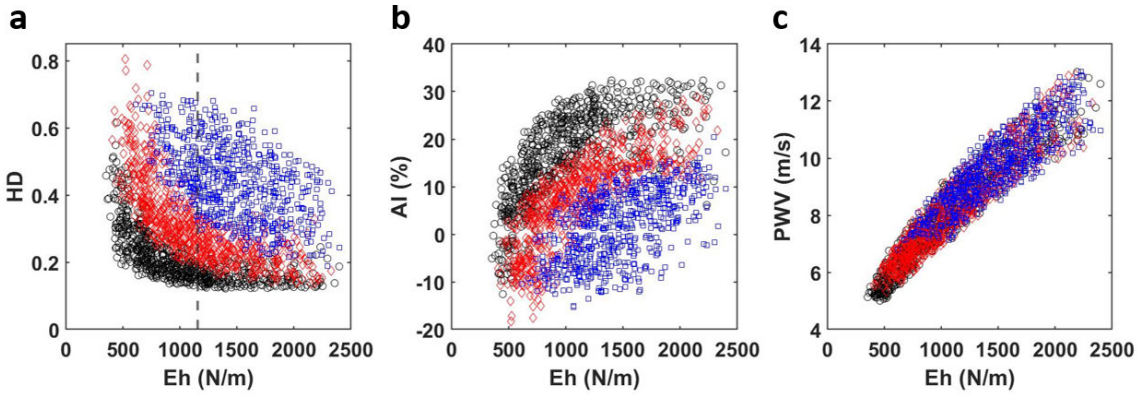

Figure 4.8: HD, AI and PWV values from randomly generated arterial trees (N = 1000) as a function of structural stiffness. Data is further visualized by scaled length. The shortest third of the data is colored black, the middle third is colored red, the longest third is colored blue. (a) harmonic distortion (HD), (b) augmentation index (AI), and (c) pulse wave velocity (PWV). The vertical dashed line at *Eh* = 1158 N/m, indicated in (a), represents the median structural stiffness.

Taking the data set of parameters and indexes from the randomly generated arterial trees, a partial correlation test was performed controlling for all parameters (vessel length, radius, viscoelastic phase, blood density, blood viscosity, as well as systolic blood pressure) but the product of modulus and thickness in order to assess sensitivity of each index to structural stiffness and each other. (Table 4.4). All indexes showed a strong correlation with *Eh*. Using the inflection point as a threshold (Figure 4.8a) the data was further divided into low and high stiffness regimes and the partial correlation test was repeated.

Table 4.4: Partial correlations using HD, AI, and PWV along with structural stiffness.

	Eh	*AI*	*PWV*
HD	-0.65	-0.90	-0.76
PWV	0.78	0.75	
AI	0.61		

Table 4.5: Partial correlations using sub-groups of HD, AI, PWV and structural stiffness.

< Eh Median

	Eh	*AI*	*PWV*
HD	-0.80	-0.89	-0.80
PWV	0.95	0.85	
AI	0.84		

> Eh Median

	Eh	*AI*	*PWV*
HD	-0.68	-0.77	-0.68
PWV	0.97	0.55	
AI	0.54		

The first column in each table, representing the three indexes' correlation coefficients with *Eh*, demonstrates mostly strong correlations with structural stiffness. The notable exception being the stiffness sub-group greater than the inflection point where AI shows a weak correlation with *Eh*. Furthermore, while in the low stiffness regime, HD's correlation with *Eh* is only marginally higher than that of AI, HD's correlation is significantly higher in the high stiffness regime.

4.5 Discussion

In this study, we constructed a transmission line model to produce BPWs that depend on the variable mechanical impedance of each major vessel in the human vasculature. Using the model, we quantified the effects of model parameters on changes in the BPW time domain morphology as well as the corresponding frequency domain features. The index HD, which we introduced and studied recently using a mouse model of aging and metabolic disease (Milkovich et al., 2022), showed promises as a measure of arterial stiffness with potential clinical applications. The model was used to study the relations of two additional cardiovascular risk indexes, AI, and PWV, to different vessel parameters. All indexes were found to be sensitive to structural stiffness, *Eh*. However, HD, an index that measures the relative distortion of a waveform with respect to a perfect sinusoid, provides a more comprehensive assessment of BPW morphology than AI by including contributions of both magnitude and arrival time of the reflected wave. Therefore, within the limitations of the transmission line model, this study reinforces HD as a useful index which is easy to implement and reliably correlates with cardiovascular risk via arterial structural stiffness.

The framework of transmission line models of cardiovascular systems has been developed decades ago (Womersley, 1957; Noordergraaf et al., 1963; Westerhof et al., 1969; Avolio, 1980; Stergiopulos et al., 1992; Ferrari et al., 2000; Davies et al., 2012; Masuda et al., 2013), and were used to study AI and PWV sensitivity (Westerhof and

Westerhof, 2012; Xiao et al., 2017a; Xiao et al., 2017b). Our study shows that AI is more sensitive to arterial stiffness than geometric parameters (Figure 4.6a), which is consistent with previous findings (Westerhof and Westerhof, 2012). It was further revealed that increased viscoelasticity of the arterial wall promotes a stronger correlation between heart rate and PWV (Xiao et al., 2017a; Xiao et al., 2017b). We also found viscoelasticity to be essential for the transmission line model to produce appropriate BPWs (not shown), although we note that viscoelasticity had little effects on the cardiovascular risk indexes (Figure 4.7a). In our study, we further examined both AI and PWV indexes as well as HD's relative sensitivity to parameters that influence the characteristic impedance of the transmission line model.

Our results demonstrated that HD is inversely related to stiffness through *Eh* (Figure 4.6a), when controlling for all other parameters, both geometric and those relating to material properties listed in Table 4.4. In clinical practice, structural stiffness is often used over the elastic modulus (Humprey et al., 2016; Mitchell et al., 2010b). The determination of the appropriate *h* required for calculating a specific *E* often is challenging. Therefore, *Eh* is used to represent the average contribution of different components within the arterial wall. Furthermore, structural stiffness is critical in understanding hemodynamics due to changes in arterial wall thickness via extracellular matrix remodeling playing a key role in vascular diseases such as hypertension (Mitchell et al., 2010b). Indeed, it is thought that structural stiffness may have a role in a positive feedback loop in conjunction with hypertension; as the arterial wall remodels it may

promote further hypertensive effects leading to more remodeling (Boutouyrie et al., 2021). Thus, structural stiffness as defined by *Eh* appears to play an essential role in cardiovascular health. The *Eh* values used in this study (Table 4.3) are consistent with previously observed clinical range of aortic *Eh* ranging from 100 to 1750 N/m (Guala et al., 2019), and with the values reported by Mitchell et al., 2003 (~ 2400 ± 900N/m in a normotensive male group). Increasing *Eh* has a dramatic effect on the evolution of BPW morphology which shows not only an increase in peak pressure, but an increasingly delayed forward wave (Figure 4.4a). Importantly, the movement of this wave promotes the aggregate BPW to transition for somewhat of a square wave to become more sinusoidal and therefore reduce HD (Figure 4.6a). Alongside increasing systolic pressure, decreasing diastolic pressure is also observed which generates larger PP values. This is likely related to the decoupled changes in parameters in the model that will lead to increased values of impedance at zero frequency.

We also noted HD's strong sensitivity to the remaining geometric vessel parameters, such as vessel length and radius, a trend that is shared by AI but in an opposite direction (Figure 4.6). Most notably vessel length, which could be thought of as analogous to human height, has the opposing effect on HD and AI. This is due to altering the reflected wave arrival and therefore waveform morphology (Figure 4.4b and Figure 4.6b). HD and AI's strong sensitivity to changes in vessel radius (Figure 4.6c) can be understood by the contribution of radius to the mechanical impedance, because both the longitudinal and transverse impedance decrease strongly with increasing radius

(Equations 4.3–4.5). Indeed, increasing radius similarly changes the waveform shape as decreasing *Eh* (Figure 4.4a and Figure 4.4c). Physiologically, low radius values are rarely reached (Table 4.3). AI's sensitivity to vessel geometry has been previously observed (Westerhof and Westerhof, 2012). From a clinical perspective, the consistent trend of AI exhibiting notably higher values in women can be interpreted as a consequence of AI tending to be elevated in individuals of shorter stature, which is associated with the presence of shorter blood vessels (Yasmin and Brown, 1999; Mitchell et al., 2004). As a result, it's logical to speculate that HD, which shares many similarities with AI (Figure 4.6), would also reflect this characteristic. However, even when studies control for height, they continue to report elevated AI values in women (Gatzka et al., 2001; Ayer et al., 2010). This persistent discrepancy is likely attributed to the presence of smaller muscular arteries in females (Benjamin, 2004; Lam et al., 2010). Further clinical study, perhaps utilizing HD alongside AI, is needed to better understand this phenomenon.

As expected, PWV remains the benchmark for accurate assessments of arterial stiffness as shown in our results the strong correlation between PWV and *Eh* (Table 4.4 and Table 4.5). A fundamentally different measure with respect to the other two indexes, PWV is a highly reliable measure of arterial stiffness that correlates strongly with various cardiovascular conditions such as aging, diabetes, and hypertension (Blacher et al., 1999; Nichols, 2005). Previously reported averages of PWV in normotensive adult males (8.2–8.7 m/s ±2 m/s) (Mitchell et al., 2003; Mitchell et al., 2004b), fall within the range of our generated values, 5–14 m/s (Figure 4.8c). Though clinical PWV can be much higher than

the maximum value generated in our study, reaching over 20 m/s for people with cardiovascular disease, the typical normotensive range of PWV (5–15 m/s) (Mitchell et al., 2004) aligns with our reported values. Notably, we observe that *Eh* plays a dominating role in determining PWV values (Figure 4.8c). Though stature could play a role in PWV (Moon et al., 2020), it is more likely that our assumption of vessel parameters scaling together promotes the PWV behavior observed in Figure 4.8c.

Our study created physiologically comparable arterial trees to mimic interindividual variability of the BPW as well as PWV seen in a clinical group. This is useful in order to study the statistical relationships in a population of non-identical arterial trees and further differentiate the three identified cardiovascular indexes. From a clinical standpoint, the similarities between HD and AI are further reflected by their correlation values with *Eh* (Table 4.4). Correlation values also change within the stiffness sub-groups (Table 4.5). HD shows further promise as a stiffness index displaying high correlation values for both stiffness sub-groups. In fact, HD shows superior correlation with *Eh* over AI in the stiffest sub-group and maintaining a similar correlation with AI in the less stiff sub-group. AI's strong correlation with *Eh* values less than the *Eh* median (Figure 4.8) can be explained by AI being a more successful stiffness index in individuals younger than 60 years of age (Mitchell et al., 2004; Mitchell et al., 2010b). In short, the results of the partial correlation test in the high stiffness sub-group imply that HD is potentially a stronger predictor of arterial stiffness in individuals with arterial stiffening. Several studies have compared AI to PWV, with contradictory findings in the correlation

of the two indexes (Lacy and Williams 2005; Sakurai et al., 2007; Mitchell et al., 2010b; Rich and Burkhoff, 2017). In our study, we found AI to correlate more poorly with PWV as compared to HD (Table 4.5). As we have discussed, HD can be sensitive to reflected wave arrival timing, while AI is not. Furthermore, true physiological waveform has noise, or waves with significant overlap, which at times has made the location of inflection points difficult to locate in AI analysis (Chen et al., 1996; Hughes et al., 2013). HD analysis, however, can be successfully applied to any complete isolated BPW.

4.6 Limitations

Due to the nature of the transmission line model, there are several assumptions to consider. First, the model assumed that all vessels scaled together, and did not fully account for the distinct effects of aging on arterial properties, such as the relatively small changes in the Young's modulus of muscular arteries compared to elastic arteries in aged population (Mitchell et al., 2010a). Future studies that allow for discontinuities between arterial segments, such as the joining of an elastic with a muscular artery, are needed. However, the generated arterial trees using our model resulted in PWV values lower than this older age group (Mitchell et al., 2010a). Therefore, arterial trees with vessel parameters analogous to an older population are not represented in this study. Additionally, the mechanical properties of the arterial wall were assumed to be linearly elastic, while nonlinear anisotropic wall mechanics have been broadly reported (Volokh, 2011; Milkovich et al., 2022). The input blood flow waveform was held constant in the model; however, HD is sensitive to the flow input. Therefore, flow morphology change

needs be taken into account by considering an individual's flow pattern over a length of time (Bessonov et al., 2016). Similarly, beat-to-beat blood pressure variability likely produce intra-subject variability of all three indexes. Blood is a non-Newtonian viscous fluid, but water properties are often used in cardiovascular studies, both computational and experimental, as an approximation to blood (Bessonov et al., 2016). The effect of perivascular pressure due to surrounding tissues on arterial properties (Ferruzzi et al., 2018b; Milkovich et al., 2022) was neglected in the current study. Wall tapering along the length of longer arteries was also neglected. Thus, input impedance was calculated by adding discrete segments with characteristic impedance that jumped at bifurcations. The ends of the transmission line model was terminated with 3-element Windkessels. However, studies have shown that the smaller distal vessels modeled by the Windkessel terminations have negligible contribution to the input impedance (Van den Wijngaard et al., 2008). Furthermore, the electrical circuit modeling of the mechanical input impedance of the vasculature (Figure 4.2) does not allow for turbulent blood flow. Future studies considering aging and diseases may need improvement of the model by considering different arrangement and number of circuits features (Jager et al., 1965; Westerhof et al., 1969).

4.7 Summary

The BPW is an often-overlooked measurement due to the intricate interaction of several confounding vessel and blood parameters. Further doubt has been cast on the BPW as a possible source of *in vivo* information pertaining to cardiovascular health from mixed and conflicting results in past studies. This study demonstrated that results relating waveform morphology to vessel properties should be obtainable in human subjects. In particular, HD has shown promise as an index to assess changes in arterial mechanical function. We further observed HD to be closely related to geometric vessel parameters, much like AI. Beyond directly correlating with stiffness, HD also correlates well with AI and PWV when controlling for all other factors. Although HD meets some limitations similar to those of other cardiovascular risk indexes, the ease of measure and the simple method of calculation make HD a potentially useful index that should be tested in a clinical setting as a means to assess cardiovascular risk.

CHAPTER 5 CARDIOVASCULAR RISK ANALYSIS VIA HUMAN BLOOD PRESSURE WAVEFORM

5.1 Overview

As cardiovascular condition change in an individual due to aging and diseases, the blood pressure waveform (BPW) tends to augment, reflecting vascular alterations. This study explores the clinical efficacy of utilizing harmonics extracted from BPWs , harmonic distortion (HD), to assess changes associated with aging and various cardiovascular risks, including diabetes, hypertension, stroke, and heart disease. BPWs from the Framingham Heart Study were noninvasively recorded using carotid artery tonometry from a diverse cohort of adults aged 19 to 89 (N = 500). Additional hemodynamic and clinical demographic information was collected. HD demonstrated a significant correlation with PWV, highlighting its sensitivity to vascular changes. Contrary to expectations, these waveforms revealed no significant correlation between the augmentation index (AI), a measure of waveform morphology, and pulse wave velocity (PWV), the established gold standard for cardiovascular risk assessment. Notably, we observed a robust correlation between HD and the presence of diabetes, suggesting that HD may be particularly responsive to conditions associated with this disease and potentially associated with left ventricular function. Furthermore, HD did not exhibit a significant correlation with heart rate, distinguishing it from other indices. This, combined with the superior statistical performance of HD over AI concerning hemodynamic variables, implies that HD may serve as a more effective measure for assessing cardiovascular risk in relation to BPW morphology. Our findings propose that

HD could be a stable and sensitive indicator for age-related vascular changes and cardiovascular risk assessment.

5.2 Introduction

Blood pressure (BP) has long been employed as a fundamental metric in assessing cardiovascular function, playing a central role in identifying hypertension (HT), a condition closely entwined with the stiffening of arterial walls (Weisbrod et al., 2013). The stiffening of central elastic vessels, such as the aorta and carotid arteries, produces a rise in pressure due to the augmentation of propagating and reflected waves, both integral components of the BP waveform (BPW) (van Varik et al., 2012). Consequently, the BPW is intricately linked to the assessment of cardiovascular risk. However, the relationship between arterial health and the intricate nuances of BP characteristics is not straightforward.

Traditional BPW indices like the augmentation index (AI) have shown limited consistency in their correlation with arterial stiffness, particularly in individuals over the age of 60 (Mitchell et al., 2004). This incongruity raises the question of whether all elements of BP responsible for distorting the BPW via wave reflection, namely both magnitude and wave phase, have been inadequately accounted for.

The association between arterial stiffness and clinical outcomes becomes increasingly evident, not to mention the accompanied complexities of aging and

cardiovascular health. With advancing age, there is a notable increase in the amplitudes of both forward and reflected pressure waves, resulting in elevated systolic and pulse pressure (Mitchell et al., 1999; Chae et al., 1999; Franklin et al., 1999; Domanski et al., 2001). These physiological changes are accompanied by a surge in pulse pressure, serving as an indirect indicator of arterial stiffness, alongside the more direct measure of carotid-femoral pulse wave velocity (PWV) (Blacher et al., 1999; Laurent et al., 2001; Nichols 2005). Arterial stiffening has been linked to several well-established cardiovascular disease risk factors, such as aging and hypertension, suggesting that it could serve as a marker for advanced atherosclerotic vascular disease (Glasser et al., 1997; Brooks et al., 1999; Blacher et al., 1999; Meaume et al., 2001).

Recent we introduced a new index, harmonic distortion (HD), derived from the BPW, which has shown promise in assessing cardiovascular risk in both animal and computational models (Milkovich et al., 2022; Milkovich et al., 2023). Building upon our previous study, we hypothesize that HD may offer perspectives complimentary to the existing indexes on characterizing arterial health within the context of clinically collected human BPWs. To investigate this hypothesis, we conducted an analysis of BPWs obtained from participants in the Framingham Heart Study (FHS), with a particular focus on the presence and implications of HD, alongside a comparison with established arterial function indices.

5.3 Material and methods

5.3.1 Collection of blood pressure waveforms

The design of the Framingham Offspring and Third Generation studies have been presented (Kannel, 1979; Splansky et al., 2007). Briefly, central pressure-flow were assessed routinely in participants undergoing their examination for the study via carotid artery tonometry (n = 500). BPWs with a duration of 10 to 20 seconds per participant were recorded noninvasively by positioning a tonometry device above the participant's skin, over the common carotid artery. Alongside this information, clinical demographic and hemodynamic data is recorded for each participant. The Boston University Medical Center Institutional Review Board approved the protocol, and all participants gave written informed consent. A satisfactory evaluation of carotid-brachial and carotid-femoral PWV was carried out in participants with complete hemodynamic data. Details of the noninvasive hemodynamic protocol and analyses have been published by Mitchell et al., 2010b (Murgo et al., 1980; Liu et al., 1986; Westerhof et al., 1972; Kelly and Fitchett 1992; Mitchell et al., 2002).

5.3.2 Blood Pressure Waveform Processing

To analyze the BPW, individual cardiac cycles were isolated, which involves an initial estimation of the BPW's interval using a custom MATLAB code. Subsequently, we calculated the first derivative of this waveform approximation and recorded the time at which the maxima occurred. The 'foot' or base of the BPW was defined as 20% of these maxima on the BPW (Mitchell et al., 2004). Once both feet of the waveform were

identified, we proceeded to compute HD and AI for each cardiac cycle. The HD formulation has been documented previously, measuring the energy above the fundamental frequency through discreet Fourier transform (DFT) of the BPW, from which the ratio of the harmonics to the fundamental frequency were calculated (Milkovich et al., 2022; Milkovich et al., 2023). AI was also calculated as the ratio of augmentation pressure to the pulse pressure of the BPW (Mitchell 2004; Milkovich et al., 2023). These individual index values were calculated for each cardiac cycle and then averaged for each participant over the 10 to 20-second interval.

If we were unable to successfully isolate individual BPWs for analysis, these participants were removed. 29 such individuals were identified with BPWs too noisy to process or an error in the data acquisition process too significant to be of use. These participants ranged in age and sex.

5.3.3 User hand tremor

During the process of collecting BPW data, it was observed that the accuracy of BP tonometry measurements might be susceptible to interference from user hand tremors. In other words, it was possible that the natural shaking or trembling of a user's hand while performing the measurements could introduce additional frequency components, known as harmonics, into the BPW data. To address this concern, the BPW transformed into the frequency domain using DFT allowed us to examine the presence of harmonics within a specific frequency range, specifically, the range of 4 to 8 Hz, which corresponds to the

typical frequency of hand tremors (Zheng et al., 2017). Within this frequency range, we calculated the total energy by squaring the DFT values and then summing them. This energy value was meticulously recorded for each participant. Subsequently, the effect of hand tremor was quantitatively defined if the energy present in the BPW data within the 4 to 8 Hz frequency range exceeded the average energy level in that band, plus one standard deviation calculated from the entire population's data.

5.3.4 Statistical analysis

In our analysis of clinical demographic and hemodynamic data, we conducted a series of correlation tests to uncover meaningful relationships between indices and hemodynamic and demographic variables. To ensure the robustness of our findings, we employed correlation test and linear regression tests. Prior to conducting statistical tests, we confirmed the normal distribution of HD and AI using the Kolmogorov–Smirnov test. To investigate whether there were significant differences in the means of HD and AI between participants with and without hand tremors, Student t-test was performed to determine whether the presence of hand tremors had a statistically significant impact on these hemodynamic parameters.

When investigating the correlation between hemodynamic parameters and cardiovascular risk indexes, we initially separated our participants by sex. Subsequently, a partial correlation test was conducted using SPSS (Chicago, IL, USA), where several critical confounding variables, including age, age squared (age2), height, weight, heart

rate (HR), high-density lipoprotein cholesterol (HDL), total cholesterol (TC), hypertension medication usage, lipid medication usage, reported diabetes (DM) and previous cardiovascular disease (CVD) were adjusted for in the analysis. This approach allowed us to discern specific relationships while minimizing the influence of potential confounders. Furthermore, when assessing correlations between cardiovascular risk indexes, the entire participant pool was analyzed while adjusted for the same key variables.

Furthermore, analysis of variance (ANOVA) test was conducted for each cardiovascular risk index (HD, AI, and PWV) to assess their significance concerning age, age2, and sex. This approach allowed us to explore potential interactions and dependencies between these factors and the hemodynamic indexes under investigation. Logistic regressions were performed on the cardiovascular events, DM, HT, and CVD, due to them being bimodal variables. In these regressions, all previously mentioned confounding factors were adjusted for, with the exception of the event in question.

Throughout our statistical analysis, we used a significance threshold of $p < 0.05$* to denote statistically significant results and $p < 0.01$** to highlight highly significant findings. These stringent criteria ensured the reliability and robustness of our conclusions.

5.4 Results

5.4.1 Blood pressure waveform characteristics

Clinical demographic characteristics of the samples are presented in Table 5.1. The subject group (n = 471) was split evenly between men and women, with women making up slightly more of the total (Table 5.1). The sample overall contains normal characteristics and approximately a quarter of the participants being treated for some form of cardiovascular condition (Lipid or HT drugs).

Table 5.1: Clinical demographic information pertaining to the FHS participant sample, delineated by sex.

Variable	Men (N = 206)	Women (N = 265)
Age, years	50 ± 16	50 ± 16
Height, cm	177 ± 7	163 ± 7
Weight, kg	88 ± 15	68 ± 14
Brachial systolic pressure, mm Hg	124 ± 14	119 ± 17
Brachial diastolic pressure, mm Hg	72 ± 9	66 ± 10
Mean arterial pressure, mm Hg	93 ± 11	88 ± 12
Central pulse pressure	121 ± 17	118 ± 19
Heart rate, bpm	56 ± 7	55 ± 6
HDL cholesterol, mg/dL	46 ± 12	60 ± 17
Total cholesterol, mg/dL	194 ± 34	193 ± 39
Lipid RX, n (%)	46 (22)	52 (20)
Hypertension RX, n (%)	25 (12)	36 (14)

Significant alterations in BPW morphology were observed with aging, as illustrated in the representative BPWs for a young (21 years old), middle-aged (51 years old), and old (81 years old) female (Figure 5.1). Notably, we observed a distinctive pattern in augmentation pressure, transitioning from negative to positive values, a phenomenon commonly observed during middle age (Figure 5.1a and Figure 5.1b). This transition is prominently represented by the distinct 'shoulder' in Figure 5.1b. Furthermore, as participants advanced in age, we noted a trend in BPWs adopting a more sinusoidal shape, leading to consistently reduced HD values. This observation underscores the progressive alterations in BPW characteristics that accompany the aging process. AI, on the other hand, rises from young to middle-aged BPW (Figure 5.1b) and then lowers again in the old BPW (Figure 5.1c).

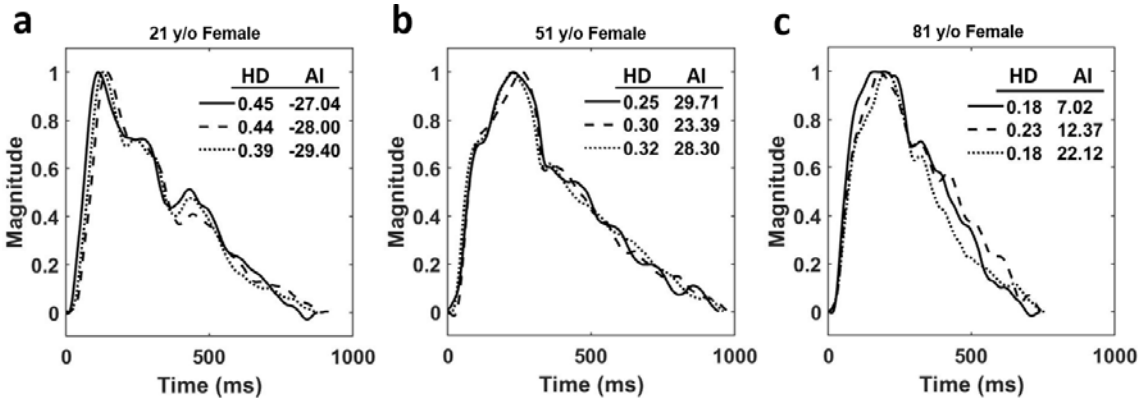

Figure 5.1: Successive isolated blood pressure waveform samples from three different female participants in the study ranging in age from (a) 21, (b) 51, and (c) 81 with their corresponding harmonic distortion and augmentation index values listed.

In accounting for the influence of hand tremor via user error in the BPW data, we found the identified participants to have hand tremor as qualified in the methods, to have no significant difference in either HD or AI with respect to participants without hand tremor.

5.4.2 Hemodynamic properties

Corresponding to the two sex sub-groups, a correlation analysis was performed adjusting for confounding factors: age, age2, height, weight, HDL, TC, hypertension and lipid medication usage, DM, CVD (Table 5.2). Hemodynamic parameters of interest were identified and correlated with cardiovascular risk indices such as systolic BP (SBP), diastolic BP (DBP), mean arterial pressure (MAP), central pulse pressure (CPP), and heart rate (HR). Correlation coefficients are listed on Table 5.2 along with the level of statistical significance. An ANOVA test performed on the correlation coefficients and the corresponding indices, it was found that PWV has significantly higher correlation values with all cardiovascular risk factors, followed by HD. Strikingly, HD was found to not significantly correlate with HR, regardless of sex.

Table 5.2: Hemodynamic correlations for the identified cardiovascular risk indices, PWV, AI and HD, by BP variables and HR. Correlations are further delineated by sex.

		Correlation Values				
Variable	**Sex**	**SBP**	**DBP**	**MAP**	**CPP**	**HR**
Carotid-femoral PWV, m/s	Male	0.329**	0.340**	0.392**	0.352**	-0.114*
	Female	0.384**	0.347**	0.403**	0.363**	-0.207**
Augmentation index, %	Male	0.151*	0.126	0.197*	0.242**	0.183*
	Female	0.193*	0.166*	0.223**	0.266**	0.233**
Harmonic Distortion, -	Male	-0.203*	-0.288**	-0.276**	-0.212*	0.022
	Female	-0.214**	-0.153*	-0.233**	-0.258**	0.109

SBP -Systolic Blood Pressure; DBP -Diastolic Blood Pressure; MAP -Mean Arterial Pressure; CPP -Central Pulse Pressure; HR -Heart Rate
*Correlations significant at the P<0.05 level **Correlations significant at the P<0.001 level

5.4.3 Cardiovascular risk indexing

The participants were further separated into evenly spaced age groups spanning twenty years: < 40, 40–59, 60–79, and > 79 years of age. The BPW indexes, HD, AI, and PWV, were averaged for these groups and plotted along with standard deviation (Figure 5.2). All indexes were found to be significantly correlated with both aging and sex. We also observe female participants to switch index direction trends in late age for both HD and AI (Figure 5.2a and Figure 5.2b). Though, this movement appears to occur later for HD when compared to AI. Male participants appear to plateau for the two indices in the same range of aging (Figure 5.2a and Figure 5.2b). In comparison, PWV values increase in a linear trend with aging for both male and female participants (Figure 5.2c).

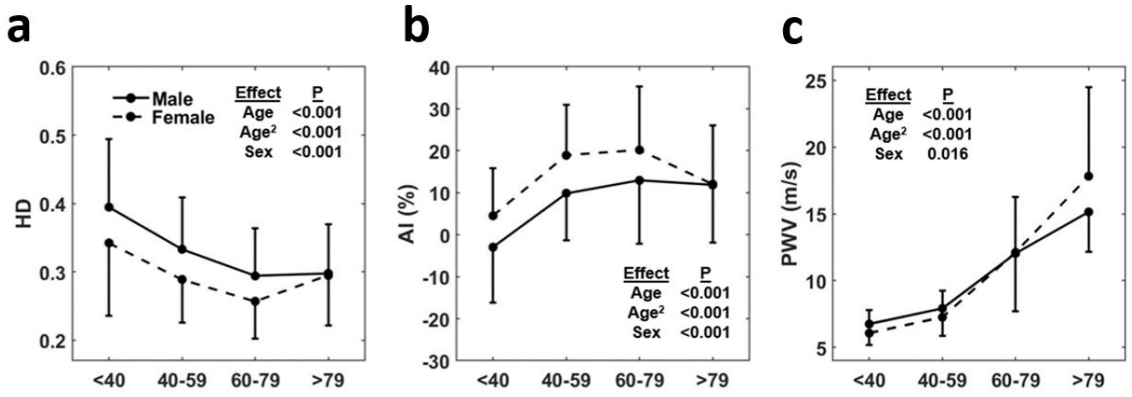

Figure 5.2: The average HD (a), AI (b), and PWV (c) values of the participants were plotted. Participants were separated by sex and age (four age groups spanning approximately 20 yrs).

5.4.4 Cardiovascular events

Cardiovascular risk indices were taken as the total population of participants for logistic regressions while adjusting for confounding factors (Table 5.3). Risk and Cardiovascular events were studied in this statistical test, namely: diabetes (DM), HT, and previous cardiovascular disease (CVD) events which includes previous instances of stroke, heart attack or heart failure. Logistic regression coefficients are listed on Table 5.3 along with the level of statistical significance. Though no significance was found between the identified risk indices and CVD, there was positive significance found with PWV and HD with respect to DM, meaning a higher index value corresponding to a higher likelihood of DM (Table 5.3). HT was also found to have positive significance with PWV and no other index (Table 5.3).

Table 5.3: Logistic regression results for the identified cardiovascular risk indices, PWV, AI and HD, by the bimodal cardiovascular events.

	DM		HT		CVD	
Variable	B	p-value	B	p-value	B	p-value
Carotid-femoral PWV, m/s	0.614	0.010	0.486	0.025	0.237	0.301
Augmentation index, %	-0.097	0.674	0.243	0.105	-0.210	0.918
Harmonic Distortion, -	0.619	0.012	-0.048	0.745	0.311	0.236

Two linear regressions were performed between PWV and HD, both adjusted from their calculated values, as well as PWV and AI (Figure 5.3). The fit R^2 value of both regressions was found to be 0.09 and 0.04 respectively. To further understand the relationship of these indices with one another, partial correlation tests were performed. For the three identified cardiovascular risk indices, the test was rerun while adjusting for all confounding factors (Table 5.4). The results of these tests demonstrate a negative weak correlation between HD and PWV as well as a negative strong correlation between HD and AI. However, no significant correlation was found between AI and PWV.

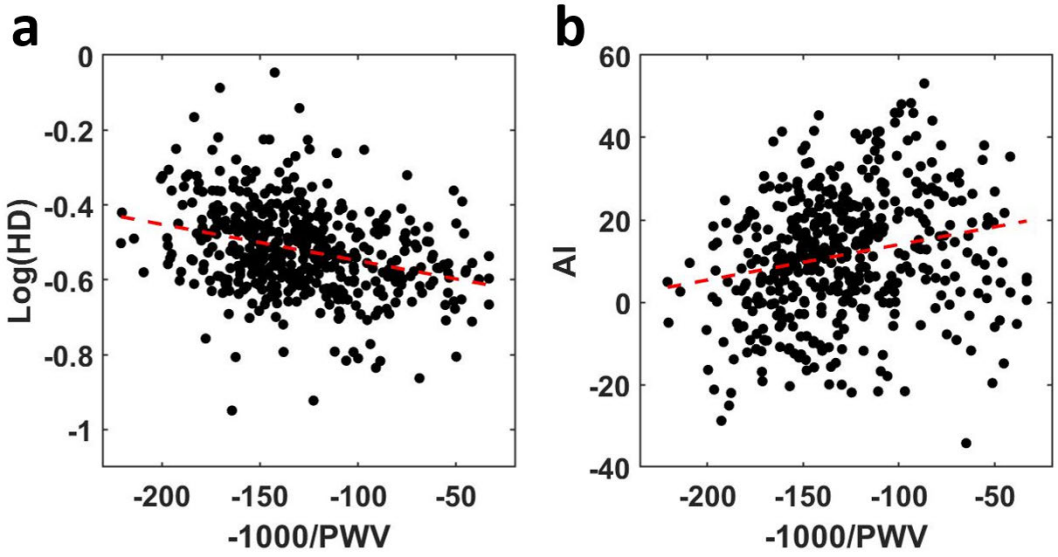

Figure 5.3: Scatter plots of adjusted PWV values (-1000/PWV) with the log of HD (a) and AI (b) along with linear regression lines R^2 = 0.09 and 0.04 respectively.

Table 5.4: Partial correlation results for the identified cardiovascular risk indices, PWV, AI and HD, by one another.

	HD		AI	
Variable	Correlation	p-value	Correlation	p-value
Carotid-femoral PWV, m/s	-0.136	0.004	0.023	0.619
Augmentation index, %	-0.489	<0.001	1.000	-
Harmonic Distortion, -	1.000	-		

5.5 Discussion

In our study, we examined a clinical sample comprising relatively healthy adult individuals. Our investigation revealed a substantial increase in age-related aortic stiffening, as quantified through carotid-femoral PWV measurements (Figure 5.3c and Table 5.3). Additionally, we made noteworthy observations concerning BPWs, shedding light on the physiological dynamics associated with aging (Figure 5.1). Strikingly, we found HD to not correlate with HR at all (Table 5.2). Further, we found our index calculated using BPW morphology, HD, to correlate significantly with hemodynamic variables and to a higher level than AI (Table 5.2). Indeed, AI, which is sensitive to changes in both the forward and reflected waves constituting the blood pressure waveform, exhibited behavior consistent with previous observation (Mitchell et al., 2004). However, AI demonstrated no correlation with PWV and other cardiovascular events. In contrast, HD displayed significant correlation with PWV, suggesting its potential as an index sensitive to age-related vascular changes. Notably, HD also exhibited a weak yet significant correlation with DM, indicating its sensitivity to the influences of metabolic syndrome.

Our investigation further delved into the relationship between these indices and hemodynamic variables: SBP, DBP, MAP, CPP, and HR. AI exhibited correlation values (Table 5.2) consistent with previously reported studies correlating AI with hemodynamic variables (Nurnberger et al., 2002; Mitchell et al., 2004b). PWV also consistently exhibited correlation values with hemodynamic parameters (Table 5.2) that aligned with

established literature, reinforcing the validity of our findings (Blacher et al., 1999; Mitchell et al., 2004b; Nichols 2005). Correlation values of HD with the same hemodynamic variables performed significantly better than AI in a paired t-test, with PWV performing the best of the three indices.

An intriguing aspect of our research was the observation that HD did not significantly correlate with HR in either sex subgroup. A few previous studies examined HR with respect to waveform morphology assessment using AI. Indeed, a study has demonstrated a significant linear relationship between AI and HR (Wilkinson et al., 2000; Sharman et al., 2009), a finding that we were able to recreate (Table 5.2). In this prior study, the inverse linear relationship was thought to be due to alterations in the timing of the reflected pressure wave, produced by changes in the absolute duration of systole (Wilkinson et al., 2000). They also noted that increased wave reflection may explain the lack of rise in central systolic pressure despite an increase in peripheral pressure (Wilkinson et al., 2000), which suggests that AI is an index with acute sensitivity to the rate at which waveforms travel. It is known that HR plays a role in the development of cardiovascular disease (Reil and Bohm 2007; Perret-Guillaume et al., 2009). Increased HR further increases PP, leading to an increase of peripheral blood pressure without showing changes in central blood pressure (Albaladejo et al., 2001; Wilkinson et al., 2002a), which can also lead to increases cardiovascular risk and HT (Albaladejo et al., 2001). The lack of correlation between HR and HD, which could be explained by HR's decoupled correlation with blood pressure and cardiovascular risk, suggests that HD may

offer distinct advantages, especially in clinical settings where participants often experience elevated HR due to the inherent anxiety associated with data collection (Light 1981; Ceconi et al., 2011).

Furthermore, we explored the age and sex differences in our chosen cardiovascular risk indices. As expected, we observed a significant increase in PWV with aging (Figure 5.3c) which is supported by previous study and implies age-based aortic stiffening (Mitchell et al., 2004; Nichols 2005). Both HD and AI, however, have nonlinear trends with increasing age (Figure 5.3a and Figure 5.3b). This is supported by our previous study in which we simulated of stiffening in the arterial tree using a transmission line model (Milkovich et al., 2023). We found both morphology indices to correlate with stiffness, which in this case can act as a substitute for aging as presented in Figure 5.3. HD has a negative nonlinear trend which converges to 0, a pure sinusoid. Notably, we observe a difference between sex for HD, with females exhibiting a slight increase in HD in late life (Figure 5.3a). This can be understood through the perspective of waveform morphology between sexes. One potential cause is the statue of females being shorter to that of males. Indeed, previous study has linked AI closely to vessel length (Yasmin 1999; Mitchell et al., 2004b; Milkovich et al., 2023). However, regardless of height, AI has been found to be higher in females (Gatzka et al., 2001; Ayer et al., 2020), suggesting waveform morphology differences between males and females. One such explanation could be smaller muscular arteries in females (Benjamin, 2004; Lam et al., 2020), causing further augmentation of the BPW. Our findings further indicate that

AI plateaued earlier in women, between the 40–59 and 60–79 age groups, whereas HD exhibited a more extended plateau, occurring much later, beyond the age of 80 (Figure 5.2a). This divergence underscores a limitation of AI as a reliable index of cardiovascular risk, particularly in predicting risk after the age of 60 as previously reported (Mitchell et al., 2004; Mitchell et al., 2010a). This phenomenon can be attributed to the distinct age-related changes in arterial properties, with muscular arteries remaining relatively stable with age while elastic arteries continue to stiffen (Mitchell et al., 2010b). This shift in the virtual reflection site further down the arterial tree results in a decrease in AI, rendering it less informative as a predictor of cardiovascular risk in older populations. With its respectively delayed nonlinear trend, HD may be less sensitive to this reflection phenomena.

We observed HD to correlate with PWV (Table 5.4 and Figure 5.3a). We have previously established a relationship between HD and PWV in both a mouse model and a computational transmission line model (Milkovich et al., 2022; Milkovich et al., 2023). It stands to reason then that our results validate these findings but with weaker significance, possibly due to the large amount of variables in a clinical studies. In contrast, AI did not display significant correlations with cardiovascular events or PWV, further underscoring its limitations in predicting cardiovascular outcomes. Previous studies have shown inconsistent results regarding the significance of AI as an index, casting doubt on its reliability (Mitchell et al., 2004; Lacy et al., 2004).

In our study, after carefully adjusting for confounding factors, we investigated the correlations of various indices with cardiovascular events. Among these indices, HD emerged as a significant indicator, exhibiting strong correlations with both PWV and DM, as shown in Table 5.3 and 5.4. The influence of DM on hemodynamics and arterial health has been extensively studied (Brooks et al., 1999; Cockcroft et al., 2000; Brooks et al., 2001; Lacy et al., 2004; Forbes et al., 2007; Tomita et al., 2007; Andersen 2010;). It is well-established that DM exacerbates atherosclerosis, leading to an increase in PWV and elevated pulse pressure (Glasser et al., 1997; Brooks et al., 1999). Type 2 DM has notable consequences on cardiovascular function, characterized by a higher augmentation of aortic systolic pressure and an unfavorable cardiac workload, which is consistent with arterial stiffening (Brooks et al., 2001). Type 1 DM has similar effects on arterial health (Brooks et al., 1999; Brooks et al., 2001). Moreover, type 2 DM is associated with impaired vascular smooth muscle sensitivity and reduced functional activity of the vascular nitric oxide systems, which are crucial for endothelial function (Williams et al., 1996). In essence, the degenerative effects of DM on hemodynamics and arterial health are multifaceted and cannot be solely attributed to arterial stiffening. This complexity is exemplified the observation that glyceryl trinitrite, a source of nitric oxide, alters waveform morphology without significantly affecting peripheral pressure, thus leaving aortic compliance largely unchanged (Murrel 1879; O'Rourke et al., 1989). This implies that the onset of DM can induce changes in waveform morphology beyond just stiffness.

When discussing waveform morphology, it is important to address the functionality of the heart's left ventricle (LV). It is well known that the LV is responsible for waveform features, namely for wave intensity as defined using pressure and flow by Ohte et al., 2003. The first peak of wave intensity reflects LV contraction and the second peak is determined by LV behavior during the time from late systole to isovolumic relaxation (Ohte et al., 2003). Further, both the LV and carotid artery structure are closely related to the shape of the central pulse waveform (Saba et al., 1993). Previous study has observed LV abnormalities in participants with type 2 DM (Dawson et al., 2005). These abnormalities change the pressure waveform produced by the LV and promote the acceleration of hypertrophy as well as HT (Grossman et al.,1992; Nicolino et al., 1995; Denardo et al., 2009). If the presence of DM in this study effected LV function in the way described, it could explain the significance with HD and DM as well (Table 5.3). Though, further study is needed to understand why this would only effect the HD index and not AI which also relies on waveform morphology for its calculation.

Notably, our findings indicate that HD did not exhibit a significant correlation with HT, which is frequently discussed in the context of arterial stiffness (Cockcroft et al., 2000; Weisbrod et al., 2013; Safar 2018; Safar et al., 2018). Since HT is defined by a marked increase in blood pressure, this raises the question of why HD does not correlate with HT while demonstrating strong correlations with all other blood pressure parameters (Table 5.2). It is expected that PWV correlates highly with HT, as this relationship has been consistently observed in clinical settings, establishing PWV as a reliable predictor

of arterial health (Mitchell et al., 2004; Weisbrod et al., 2018). In this field, there is an ongoing study regarding whether arterial stiffening precedes high blood pressure or if high blood pressure contributes to the onset of arterial stiffening (Herrera et al., 2014; Weisbrod et al., 2018). Both factors play a cyclical role with each other. The disparity between the significance of HD in relation to blood pressure and its lack of significance with HT may suggest that HD may not directly measure arterial stiffness. Alternatively, it may be sensitive to the coupled effects of arterial stiffness and hemodynamic changes. However, HD could serve as an indicator of increased cardiovascular risk associated with high PWV values and the onset of DM.

5.6 Limitations

The limitations of this study are worth noting, primarily stemming from the absence of follow-up BPWs in a multi-generational context. Ideally, to provide a more comprehensive understanding of changes in BPW morphology over time, data collection in subsequent years would be essential. Such long-term data acquisition would facilitate investigations into the aging process among participants and further exploration of cardiovascular events. However, it's crucial to acknowledge that this study still offers valuable insights into participants' cardiovascular health, albeit within certain constraints. Specifically, CVD serves as a parameter that factors in prior cardiovascular conditions such as strokes, heart attacks, or heart failures. While this parameter indirectly allows for an assessment of how previous cardiovascular events might impact waveform morphology, it lacks the information regarding the timing of these events. It's important

to recognize that arterial remodeling and the restoration of arterial elasticity can be influenced by various factors, including prescription medications and lifestyle changes (Tabaka and Safar 2005; Avolio 2013). These factors may reverse the effects of previous arterial modifications, further highlighting the need for longitudinal data. To overcome these limitations and gain a more comprehensive understanding of the subject matter, future studies should aim to collect follow-up BPWs from participants, enabling a more in-depth exploration of changes in BPW morphology over time and their relationship with cardiovascular health.

5.7 Summary

We investigated various cardiovascular risk indices with a particular focus on age-related changes and their reliability in assessing vascular health. Our findings revealed a substantial increase in age-related aortic stiffening, as quantified through carotid-femoral PWV measurements. Notably, we observed significant differences between two key indices, HD and AI, in terms of their variability, with HD exhibiting greater stability. Our research also unveiled intriguing correlations between these indices and hemodynamic variables, where AI's failure to consistently correlate with systolic and diastolic blood pressure raised concerns about its robustness as an indicator of vascular health. Moreover, our study shed light on the distinctive trends of HD and AI with increasing age, highlighting AI's limitations as a predictor of cardiovascular risk, particularly in older populations. HD, on the other hand, presented a more delayed nonlinear trend, potentially making it less sensitive to age-related vascular changes.

Furthermore, we observed that HD showed strong correlations with PWV and DM, emphasizing its potential as an indicator of increased cardiovascular risk. These findings collectively contribute to a deeper understanding of the intricacies of vascular health assessment and the potential advantages of using HD as a more stable and reliable index, particularly in clinical settings where precise measurements are paramount.

CHAPTER 6 CONCLUSIONS AND OUTLOOK

6.1 Conclusions

In this study, encompassing the interactions of BPW wave propagation, arterial wall mechanics, and hemodynamics, we proposed a new index, HD, that holds immense promise for assessing changes in arterial mechanical function. Derived from the Fourier transform of individual BPWs, HD not only demonstrates a significant relationship with SBP but also exhibits sensitivity to age and metabolic syndrome-induced alterations in BPW. Notably, the accessibility of instruments used to record BPWs in clinical settings positions HD as a noninvasive and easily deployable means to evaluate cardiovascular risk.

Using a transmission line model, we studied HD as a validated index for evaluating arterial mechanical function, and demonstrated its close association with geometric vessel parameters and its correlation with established arterial stiffness measures such as AI and PWV. While sharing some limitations with other cardiovascular risk indices, the simplicity of HD's calculation and ease of measurement enhance its potential as a valuable clinical measure for cardiovascular risk assessment.

Using human BPWs collected noninvasively through the Framingham Heart Study, our investigation into various cardiovascular risk indices revealed age-related aortic stiffening, as quantified by carotid-femoral PWV measurements. Notably, HD emerged as a more stable index compared to AI, demonstrating greater reliability in

assessing vascular health. The study further unraveled distinctive age-related trends, indicating that AI's limitations as a predictor of cardiovascular risk become pronounced in older populations, while HD presents a delayed nonlinear trend, potentially making it less sensitive to age-related vascular changes.

Moreover, correlations between HD and PWV, as well as its association with DM, underscore its potential as an indicator of cardiovascular risk. Further studies are still needed to understand HD and other cardiovascular risk, such as HT and HR. Collectively, these findings contribute to current understandings of vascular health assessment, positioning HD as a new BPW index with substantial advantages, particularly in clinical settings where precise measurements are crucial.

6.2 Outlook

Our study pointed out the importance of comprehensive BPW analysis as a potential index of cardiovascular health. The introduction of the noninvasive BPW morphology index, HD, establishes a consistent correlation with elevated cardiovascular risk, opening avenues for a deeper exploration of intricate waveform interactions within the arterial tree.

The insights gained from HD, observed across both mouse and human models, coupled with its successful clinical application, highlight the versatility and repeatability of HD as a reliable index for assessing vascular health. Notably, HD's adaptability

renders it easily implementable in various environments, further enhancing its practicality. Importantly, the accessibility of the equipment and analysis required for HD underscores its feasibility for widespread use.

To enhance the analysis of HD data, future research could incorporate advanced models of human vasculature. Specifically, concerning the transmission line model introduced in Chapter 4, several novel approaches can be implemented to conduct a more nuanced analysis of the BPW under diverse conditions. Initially, the existing transmission line model fails to adequately capture the nonlinear effects of the arterial wall as they present physiologically. One potential approach involves treating arterial compliance as a function of BP, resulting in varying stiffness values for each BPW. Alternatively, a machine learning approach could be explored, wherein arterial trees and their nonlinear properties are influenced by a combination of clinical demographic information and waveforms, such as the data collected from the FHS in Chapter 5.

The significance of such prospective investigations is important, given the current limitation of the model in accounting for aging. Specifically, the differential material properties between muscular and elastic arteries introduce complexities in wave reflections at their junction (Mitchell et al., 2010). An enhanced model should distinguish between these vessel types using separate material variables. Alternatively, efforts can be directed towards identifying improved methods for transitioning between muscular and elastic vessels, a critical factor affecting the modeling of elderly individuals (Mitchell et

al., 2010). Furthermore, replacing the current assumption of scaled growth with realistic growth patterns would facilitate a more nuanced examination of how waveform harmonics evolve in a controlled environment (Westerhof et al., 2020).

Additionally, our findings underscore the sensitivity of HD to flow waveforms, prompting a need for further exploration to understand the significance of the original unimpeded waveform in the final calculation. Future research endeavors should encompass various types of waveforms, including those observed under normotensive conditions as well as hypotensive and diabetic flow waveforms.

BIBLIOGRAPHY

Ageenkova, O.A. and Purygina, M.A. (2011). Central Aortic Blood Pressure, Augmentation Index, and Reflected Wave Transit Time: Reproducibility and Repeatability of Data Obtained by Oscillometry. *Vascular Health and Risk Management 7*, 649–656.

Albaladejo, P., Copie, X., Boutouyrie, P., Laloux, B., Déclère, A. D., Smulyan, H., and Bénétos, A. (2001). Heart rate, arterial stiffness, and wave reflections in paced patients. *Hypertension, 38*(4), 949–952.

Amin, M., Le, V. P., and Wagenseil J. E. (2012). Mechanical Testing of Mouse Carotid Arteries: From Newborn to Adult. *Journal of Visualized Experiments: JoVE, 60*, 3791–3733.

Andersen, C. A. (2010). Noninvasive assessment of lower-extremity hemodynamics in individuals with diabetes mellitus. *Journal of the American Podiatric Medical Association, 100*(5), 406–411.

Avolio, A. P. (1980). Multi-branched model of the Human Arterial System. *Medical & Biological Engineering & Computing, 18*(6), 709–718.

Ayer, J. G., Harmer, J. A., Marks, G. B., Avolio, A., and Celermajer, D. S. (2010). Central Arterial Pulse Wave augmentation is greater in girls than boys, independent of height. *Journal of Hypertension, 28*(2), 306–313.

Baek, S., Gleason, R., Rajagopal, K.R., and Humphrey, J.D. (2007). Theory of small on large: Potential utility in computations of fluid–solid interactions in arteries. *Computer Methods in Applied Mechanics and Engineering. 196*, 3070–3078.

Benjamin, E. J. (2004). Clinical correlates and heritability of flow-mediated dilation in the community: the Framingham Heart Study. *Circulation, 109*(5), 613–619.

Bessonov, N., Sequeira, A., Simakov, S., Vassilevskii, Y., and Volpert, V. (2016). Methods of blood flow modelling. *Mathematical Modelling of Natural Phenomena, 11*(1), 1–25.

Blacher, J., Asmar, R., Djane S., London, G.M., and Safar, M.E. (1999). Aortic pulse wave velocity as a marker of cardiovascular risk in hypertensive patients. *Hypertension 33*, 1111–1117.

Boutouyrie, P., Chowienczyk, P., Humphrey, J.D., Mitchell, G.F. (2021). Arterial Stiffness and Cardiovascular Risk in Hypertension. *Circulation Research, 128*(7), 864–886.

Brooks, B. A., Molyneaux, L.M., and Yue, D.K. (1999). Augmentation of Central Arterial Pressure in Type 1 Diabetes. *Diabetes Care 22*, 1722–1727.

Brooks, B. A., Molyneaux, L.M., and Yue, D.K. (2001). Augmentation of Central Arterial Pressure in Type 2 Diabetes. *Diabetic Medicine 18*, 374–380.

Bundy, J. D., Li, C., Stuchlik, P., Bu, X., Kelly, T. N., Mills, K. T., ... and He, J. (2017). Systolic blood pressure reduction and risk of cardiovascular disease and mortality: a systematic review and network meta-analysis. *JAMA Cardiology*, *2*(7), 775–781.

Burattini, R., Knowlen, G. G., and Campbell, K. B. (1991). Two arterial effective reflecting sites may appear as one to the heart. *Circulation Research, 68*(1), 85–99.

Cecelja, Marina, and Philip Chowienczyk. (2009). Dissociation of aortic pulse wave velocity with risk factors for cardiovascular disease other than hypertension: a systematic review. *Hypertension 54(*6) 1328–1336.

Ceconi, C., Guardigli, G., Rizzo, P., Francolini, G., and Ferrari, R. (2011). The heart rate story. *European Heart Journal Supplements, 13*(suppl_C), C4–C13.

Chae, C. U., Pfeffer, M. A., Glynn, R. J., Mitchell, G. F., Taylor, J. O., and Hennekens, C. H. (1999). Increased pulse pressure and risk of heart failure in the elderly. *JAMA: The Journal of the American Medical Association, 281*(7), 634–643.

Chaturvedi, N. (2007). The burden of diabetes and its complications: trends and implications for intervention. *Diabetes Research and Clinical Practice, 76*, S3–12.

Chen, C., Ting, C., Nassbacher, A., Nevo, E., Kass, D.A., Pak, P., Wang, S., Chang, M., Yin, F.C.P. (1996). Validation of Carotid Artery Tonometry as a Means of Estimating Augmentation Index of Ascending Aortic Pressure. *Hypertension, 27*(2), 168–175.

Chow, M.J., Turcotte, R., Lin, C.P., and Zhang, Y. (2014). Arterial extracellular matrix: a mechanobiological study of the contributions and interactions of elastin and collagen. *Biophysical Journal, 106*, 2684–2692.

Cockcroft, J. R., Webb, D. J., and Wilkinson, I. B. (2000). Arterial stiffness, hypertension and diabetes mellitus. *Journal of Human Hypertension, 14*(6), 377–380.

Cruickshank, K., Riste, L., Anderson, S. G., Wright, J. S., Dunn, G., & Gosling, R. G. (2002). Aortic pulse-wave velocity and its relationship to mortality in diabetes and glucose intolerance: an integrated index of vascular function? *Circulation*, *106*(16), 2085–2090.

Dabasia, P. L., Lawrenson, J. G., and Murdoch, I. E. (2016). Evaluation of a new rebound tonometer for self-measurement of intraocular pressure. *British Journal of Ophthalmology, 100*(8), 1139–1143.

Davies, J. E., Alastruey, J., Francis, D. P., Hadjiloizou, N., Whinnett, Z. I., Manisty, C. H., et al. (2012). Attenuation of wave reflection by wave entrapment creates a "horizon effect" in the human aorta. *Hypertension, 60*(3), 778–785.

Dawson, A., Morris, A. D., and Struthers, A. D. (2005). The epidemiology of left ventricular hypertrophy in type 2 diabetes mellitus. *Diabetologia, 48*, 1971–1979.

Denardo, S. J., Nandyala, R., Freeman, G. L., Pierce, G. L., and Nichols, W. W. (2010). Pulse wave analysis of the aortic pressure waveform in severe left ventricular systolic dysfunction. *Circulation: Heart Failure, 3*(1), 149–156.

Domanski, M., Norman, J., Wolz, M., Mitchell, G., and Pfeffer, M. (2001). Cardiovascular risk assessment using pulse pressure in the first national health and nutrition examination survey (NHANES I). *Hypertension, 38*(4), 793–797.

Feng, M. and Keith, D. (2009). Non-Invasive Blood Pressure Measurement in Mice. *Methods in Molecular Biology 573*, 45–55.

Ferrari, G., Nicoletti, A., De Lazzari, C., Clemente, F., Tosti, G., Guaragno, M., et al. (2000). A physical model of the human systemic arterial tree. *The International Journal of Artificial Organs, 23*(9), 647–657.

Ferruzzi, J., Bersi, M.R., and Humphrey, J.D. (2013). Biomechanical phenotyping of central arteries in health and disease: advantages of and methods for murine models. *Annals of Biomedical Engineering, 41*, 1311–1330.

Ferruzzi, J., Madziva, D., Caulk, A. W., Tellides, G., and Humphrey, J. D. (2018). Compromised mechanical homeostasis in arterial aging and associated cardiovascular consequences. *Biomechanics and Modeling in Mechanobiology, 17*(5), 1281–1295.

Ferruzzi, J., Di Achille, P., Tellides, G., and Humphrey, J.D. (2018). Combining in Vivo and in Vitro Biomechanical Data Reveals Key Roles of Perivascular Tethering in Central Artery Function. *PLoS ONE 13*, 1–21.

Forbes, J. M., Fukami, K., and Cooper, M. E. (2007). Diabetic nephropathy: Where hemodynamics meets metabolism. *Experimental and Clinical Endocrinology & Diabetes, 115*(02), 69–84.

Franklin, S. S., Khan, S. A., Wong, N. D., Larson, M. G., and Levy, D. (1999). Is pulse pressure useful in predicting risk for coronary heart disease? The Framingham Heart Study. *Circulation, 100*(4), 354–360.

Fung, P., Dumont, G., Ries, C., Mott, C., and Ansermino, M. (2004). Continuous noninvasive blood pressure measurement by pulse transit time. *IEEE, IEMBS'04. 26th Annual International Conference of the IEEE*, 2239–2242.

Gatzka, C.D., Kingwell, B.A., Cameron, J.D., Berry, K.L., Liang, Y., Dewar, E.M., et al. (2001). Gender Differences in the Timing of Arterial Wave Reflection beyond Differences in Body Height. *Journal of Hypertension 19*, 2197–2203.

Gkousioudi, A., Yu, X., Ferruzzi, J., Qian, J., Wainford, R., Seta, F., et al. (2022). Biomechanical Properties of Mouse Carotid Arteries with Diet-Induced Metabolic Syndrome and Aging. *Frontiers in Bioengineering and Biotechnology, 10*, 862996.

Glasser, S.P., Arnett, D.K., McVeigh, G.E., Finkelstein, S.M., Bank, A.J., Morgan, D.J., et al. (1997). Vascular compliance and cardiovascular disease: a risk factor or a marker? *American Journal of Hypertension, 10*, 1175–1189.

Goshy, M., Lai-Fook, S.J., and Hyatt, R.E. (1979). Perivascular Pressure Measurements by Wick-Catheter Technique in Isolated Dog Lobes. *Journal of Applied Physiology, 46*, 950–955.

Grossman, E., Shemesh, J., Shamiss, A., Thaler, M., Carroll, J., and Rosenthal, T. (1992). Left ventricular mass in diabetes-hypertension. *Archives of Internal Medicine, 152*(5), 1001–1004.

Guala, A., Rodriguez-Palomares, J., Dux-Santoy, L., Teixido-Tura, G., Maldonado, G., Galian, L., Huguet, M., et al. (2019). Influence of Aortic Dilation on the Regional Aortic Stiffness of Bicuspid Aortic Valve Assessed by 4-Dimensional Flow Cardiac Magnetic Resonance. *JACC: Cardiovascular Imaging, 12*(6), 1020–1029.

Haidar, M. A., Van Buchem, M. A., Sigurdsson, S., Gotal, J. D., Gudnason, V., Launer, L. J., and Mitchell, G. F. (2021). Wave reflection at the origin of a first-generation branch artery and Target Organ Protection. *Hypertension, 77*(4), 1169–1177.

Hayashi, K., Mani, V., Nemade, A., Aguiar, S., Postley, J.E., Fuster, V., et al. (2010). Variations in atherosclerosis and remodeling patterns in aorta and carotids. *Journal of Cardiovascular Magnetic Resonance 12*, 10.

Hayward, C.S. and Kelly, R.P. (1997). Gender-Related Differences in the Central Arterial Pressure Waveform. *Journal of the American College of Cardiology 30*, 1863–1871.

Herrera, V. L., Decano, J. L., Giordano, N., Moran, A. M., & Ruiz-Opazo, N. (2014). Aortic and carotid arterial stiffness and epigenetic regulator gene expression changes precede blood pressure rise in stroke-prone Dahl salt-sensitive hypertensive rats. *PLoS One*, *9*(9), e107888.

Hirata, K., Kawakami, M., and O'Rourke, M. F. (2006). Pulse wave analysis and Pulse Wave velocity a review of Blood Pressure Interpretation 100 years after Korotkov. *Circulation Journal, 70*(10), 1231–1239.

Hughes, A.D., Park. C., Davies, J., Francis, D., Thom, S.A., Mayet, J., Parker, K.H. (2013). Limitations of augmentation index in the assessment of wave reflection in normotensive healthy individuals. *PLoS One, 8*(3):e59371.

Humprey, J.D., Harrison, D.G., Figueroa C.A., Lacolley, P., Laurent, S. (2016). Central Artery Stiffness in Hypertension and Aging: A Problem With Cause and Consequence. *Circulation Research, 118*, 379–381.

Imsirovic, J., Bartolák-Suki, E., Jawde, S., Parameswaran, H., and Suki, B. (2018). Blood pressure-induced physiological strain variability modulates wall structure and function in aorta rings. *Physiological Measurement, 39*, 105014.

Jager, G. N., Westerhof, N., and Noordergraaf, A. (1965). Oscillatory flow impedance in electrical analog of arterial system: Representation of Sleeve Effect and Non-Newtonian Properties of Blood. *Circulation Research, 16*(2), 121–133.

Jeroncic, A., Gunjaca, G., Mrsic, D. B., Mudnic, I., Brizic, I., Polasek, O., and Boban, M. (2016). Normative equations for central augmentation index: assessment of inter-population applicability and how it could be improved. *Scientific Reports, 6*(1), 27016.

Jerrard-Dunne, P., Mahmud, A., and Feely, J. (2008). Ambulatory arterial stiffness index, pulse wave velocity and augmentation index – interchangeable or mutually exclusive measures? *Journal of Hypertension, 26*(3), 529–534.

Kannel, W. B. (1979). An investigation of coronary heart disease in families. The Framingham offspring study. *American Journal of Epidemiology, 110*, 281–290.

Kannel, W. B. (2000). Elevated systolic blood pressure as a cardiovascular risk factor. *American Journal of Cardiology 2*, 251–255.

Kannel, W. B., Vasan, R. S., and Levy, D. (2003). Is the relation of systolic blood pressure to risk of cardiovascular disease continuous and graded, or are there critical values? *Hypertension 42*, 453–456.

Kelly, R and Fitchett, D. (1992). Noninvasive determination of aortic input impedance and external left ventricular power output: a validation and repeatability study of a new technique. *Journal of the American College of Cardiology, 20*, 952–963.

Kenner, T. (1989). The Measurement of Blood Density and Its Meaning. *Basic Research in Cardiology, 84*(2), 111–124.

Kim, J., Peruski, B., Hunley, C., Kwon, S., and Baek, S. (2013). Influence of Surrounding Tissues on Biomechanics of Aortic Wall. *International Journal of Experimental and Computational Biomechanics 2*, 105–107.

Kim, J., Song, T. J., Song, D., Lee, K. J., Kim, E. H., Lee, H. S., ... & Heo, J. H. (2014). Brachial-ankle pulse wave velocity is a strong predictor for mortality in patients with acute stroke. *Hypertension*, *64*(2), 240–246.

Lacy, P. S., O'Brien, D. G., Stanley, A. G., Dewar, M. M., Swales, P. P., and Williams, B. (2004). Increased pulse wave velocity is not associated with elevated augmentation index in patients with diabetes. *Journal of Hypertension, 22*(10), 1937–1944.

Lacy, P. and Williams, B. (2005). Increased pulse wave velocity is not associated with elevated augmentation index in patients with diabetes. *Journal of Hypertension, 23*(3), 670–671.

Lam, C. S., Xanthakis, V., Sullivan, L. M., Lieb, W., Aragam, J., Redfield, M. M., et al. (2010). Aortic root remodeling over the adult life course: longitudinal data from the Framingham Heart Study. *Circulation, 122*(9), 884–890.

Laurent, S., Boutouyrie, P., Asmar, R., Gautier, I., Laloux, B., Guize, L., et al. (2001). Aortic stiffness is an independent predictor of all-cause and cardiovascular mortality in hypertensive patients. *Hypertension, 37*(5), 1236–1241.

Laurent, S., Tropeano, A. I., & Boutouyrie, P. (2006). Pulse pressure reduction and cardiovascular protection. *Journal of Hypertension, 24*, S13–S18.

Liao, D., Cooper, L., Cai, J., Toole, J., Bryan, N., Burke, G., ... and Heiss, G. (1997). The prevalence and severity of white matter lesions, their relationship with age, ethnicity, gender, and cardiovascular disease risk factors: the ARIC Study. *Neuroepidemiology*, *16*(3), 149–162.

Light, K. C. (1981). Cardiovascular responses to effortful active coping: Implications for the role of stress in hypertension development. *Psychophysiology, 18*(3), 216–225.

Loehr, L.R., Meyer, M.L., Poon, A.K., Selvin, E., Palta, P., Tanaka, H., et al. (2016). Prediabetes and Diabetes Are Associated with Arterial Stiffness in Older Adults: The ARIC Study. *American Journal of Hypertension, 29*, 1038–1045.

Lowe, G.D., Drummond, M.M., Lorimer, A.R., Hutton, I., Forbes, C.D., Prentice, C.R., Barbenel, J.C. (1980). Relation between Extent of Coronary Artery Disease and Blood Viscosity. *BMJ: British Medical Journal, 280*(6215), 673–674.

Masuda, M., Emoto, T., Suzuki, A., Akutagawa, M., Kitawaki, T., Kitaoka, K., et al. (2013). Evaluation of blood flow velocity waveform in common carotid artery using multi-branched arterial segment model of human arteries. *Biomedical Signal Processing and Control, 8*(6), 509–519.

McEniery, C. M., Yasmin, N., Hall, I. R., Qasem, A., Wilkinson, I. B., Cockcroft, J. R., & ACCT Investigators. (2005). Normal vascular aging: differential effects on wave reflection and aortic pulse wave velocity: the Anglo-Cardiff Collaborative Trial (ACCT). *Journal of the American College of Cardiology*, *46*(9), 1753–1760.

Meaume, S., Benetos, A., Henry, O. F., Rudnichi, A., and Safar, M. E. (2001). Aortic pulse wave velocity predicts cardiovascular mortality in subjects> 70 years of age. *Arteriosclerosis, Thrombosis, and Vascular Biology, 21*(12), 2046–2050.

Meguro, T., Nagatomo, Y., Nagae, A., Seki, C., Kondou, N., Shibata, M., & Oda, Y. (2009). Elevated arterial stiffness evaluated by brachial-ankle pulse wave velocity is deleterious for the prognosis of patients with heart failure. *Circulation Journal*, *73*(4), 673–680.

Miao, C.Y. and Su, D.F. (2002). The importance of blood pressure variability in rat aortic and left ventricular hypertrophy produced by sinoaortic denervation, *Journal of Hypertension, 20*, 1865–1872.

Milkovich, N., Gkousioudi, A., Seta, F., Suki, B., and Zhang, Y. (2022). Harmonic distortion of blood pressure waveform as a measure of arterial stiffness. *Frontiers in Bioengineering and Biotechnology, 10,* 842754. https://doi.org/10.3389/fbioe.2022.842754

Milkovich, N., Mitchell, G.F., Suki, B., Zhang, Y. (Submitted 2023) Blood Pressure Waveform Morphology Assessed using Transmission Line Model and Harmonic Distortion Analysis.

Mitchell, G.F., Izzo, J.L., Lacourcière, Y., Ouellet, J., Neutel, J., Qian, C., et al. (2002). Omapatrilat reduces pulse pressure and proximal aortic stiffness in patients with systolic hypertension: results of the conduit hemodynamics of omapatrilat international research study. *Circulation 105*, 2955–2961.

Mitchell, G.F., Lacourcière, Y., Ouellet, J., Izzo, J.L., Neutel, J., Kerwin, L.J., Block, A.J., Pfeffer, M.A. (2003). Determinants of Elevated Pulse Pressure in Middle-Aged and Older Subjects with Uncomplicated Systolic Hypertension. *Circulation, 108*(13), 1592–1598.

Mitchell, G. F. (2004). Increased aortic stiffness: an unfavorable cardiorenal connection. *Hypertension, 43*(2), 151–153.

Mitchell, G. F., Parise, H., Benjamin, E. J., Larson, M. G., Keyes, M. J., Vita, J. A., ... & Levy, D. (2004). Changes in arterial stiffness and wave reflection with advancing age in healthy men and women: the Framingham Heart Study. *Hypertension*, *43*(6), 1239–1245.

Mitchell, G. F. (2008). Clinical achievements of impedance analysis. *Medical & Biological Engineering & Computing, 47*(2), 153–163.

Mitchell, G.F., Conlin, P.R., Dunlap, M.E., Lacourcière, Y., Arnold, J., Ogilvie, R.I., et al. (2008). Aortic Diameter, Wall Stiffness, and Wave Reflection in Systolic Hypertension. *Hypertension 51*, 105–111.

Mitchell, G.F. (2009). Arterial Stiffness and Wave Reflection: Biomarkers of Cardiovascular Risk. *Artery Research, 3*(2), 56.

Mitchell, G.F., Hwang, S., Vasan, R.S., Larson, M.G., Pencina, M.J., Hamburg, N.M., Vita, J.A., Levy, D., Benjamin, E.J. (2010). Arterial Stiffness and Cardiovascular Events. *Circulation, 121*(4), 505–511.

Mitchell, G.F., Wang, N., Palmisano, J.N., Larson, M.G., Hamburg, N.M., Vita, J.A., Levy, D., Benjamin, E.J., Vasan, R.S. (2010). Hemodynamic correlates of blood pressure across the adult age spectrum: noninvasive evaluation in the Framingham Heart Study. *Circulation, 122*(14), 1379–1386.

Moon, J., Hwang, I.C., Han, S.H. (2020). Short stature is associated with higher pulse wave velocity in subjects without overt cardiovascular disease. *Medicine, 99*(39), e22219.

Murgo, J. P., Westerhof, N. I. C. O., Giolma, J. P., and Altobelli, S. A. (1980). Aortic input impedance in normal man: relationship to pressure wave forms. *Circulation, 62*(1), 105–116.

Murrell, W. (1879). Nitroglycerine as a remedy for angina pectoris. *The Lancet, 80*, 80–81.

Nichols, W.W. and O'Rourke M.F. (1998). Chapter 9. Wave Reflections. In: *McDonald's Blood Flow in Arteries: Theoretical, Experimental and Clinical Principles*. London: Arnold, pp. 203–222.

Nichols, W. (2005). Clinical measurement of arterial stiffness obtained from noninvasive pressure waveforms. *American Journal of Hypertension, 18*, 3–10.

Nicolina, A., Longobardi, G., Furgi, G., Rossi, M., Zoccolillo, N., Ferrara, N., and Rengo, F. (1995). Left ventricular diastolic filling in diabetes mellitus with and without hypertension. *American Journal of Hypertension, 8*(4), 382–389.

Noordergraaf, A., Verdouw, P. D., and Boom, H. B. (1963). The use of an analog computer in a circulation model. *Progress in Cardiovascular Diseases, 5*(5), 419–439.

Nurnberger, J., Keflioglu-Scheiber, A., Saez, A. M. O., Wenzel, R. R., Philipp, T., and Schäfers, R. F. (2002). Augmentation index is associated with cardiovascular risk. *Journal of Hypertension, 20*(12), 2407–2414.

Ohte, N., Narita, H., Sugawara, M., Niki, K., Okada, T., Harada, A., et al. (2003). Clinical usefulness of carotid arterial wave intensity in assessing left ventricular systolic and early diastolic performance. *Heart and Vessels, 18*, 107–111.

O'Rourke, M. F., Kelly, R. P., Avolio, A. P., and Hayward, C. S. (1989). Effects of arterial dilator agents on central aortic systolic pressure and on left ventricular hydraulic load. *The American Journal of Cardiology, 63*(1), 38–44.

O'Rourke, M. F., O'Brien, C., and Edelman, E. R. (2016). Arterial Stiffening in Perspective: Advances in Physical and Physiological Science Over Centuries. *American Journal of Hypertension, 29*, 785–791.

Perret-Guillaume, C., Joly, L., and Benetos, A. (2009). Heart rate as a risk factor for cardiovascular disease. *Progress in Cardiovascular Diseases, 52*(1), 6–10.

Reddy, A.K., Li, Y., Pham, T.T., Ochoa, L.N., Treviño, M.T., Hartley, C.J., et al. (2003). Measurement of aortic input impedance in mice: effects of age on aortic stiffness. *American Journal of Physiology. Heart and Circulatory Physiology. 285*, 1464–1470.

Redheuil, A., Yu, W., Mousseaux, E., Harouni, A.A., Kachenoura, N., Wu, C.O., Bluemke, D., Lima, J.A.C. (2011). Age-Related Changes in Aortic Arch Geometry: Relationship with Proximal Aortic Function and Left Ventricular Mass and Remodeling. *Journal of the American College of Cardiology, 58*(12), 1262–1270.

Reil, J. C., and Böhm, M. (2007). The role of heart rate in the development of cardiovascular disease. *Clinical Research in Cardiology, 96*(9), 585–592.

Rich, J.D., and Burkhoff, D. (2017). Hvad Flow Waveform Morphologies: Theoretical Foundation and Implications for Clinical Practice. *ASAIO Journal, 63*(5), 526–535.

Rizzoni D, Porteri E, Boari GE, De Ciuceis C, Sleiman I, Muiesan ML, Castellano M, Miclini M, Agabiti-Rosei E. (2003). Prognostic significance of small-artery structure in hypertension. *Circulation, 108*, 2230–2235.

Roman, M. J., Ganau, A., Saba, P. S., Pini, R., Pickering, T. G., and Devereux, R. B. (2000). Impact of arterial stiffening on left ventricular structure. *Hypertension, 36*(4), 489–494.

Rucka, D., Marek, J., Rucklova, Z., Lubanda, J.C., Havranek, S., Skvaril, J., et al. (2015). Arterial stiffening contributes to impairment of cerebrovascular reactivity in patients with coronary artery disease without carotid stenosis. *Physiological Research, 64*, 335–343.

Saba, P. S., Roman, M. J., Pini, R., Spitzer, M., Ganau, A., and Devereux, R. B. (1993). Relation of arterial pressure waveform to left ventricular and carotid anatomy in normotensive subjects. *Journal of the American College of Cardiology, 22*(7), 1873–1880.

Safar, M. E., Levy, B. I., and Struijker-Boudier, H. (2003). Current perspectives on arterial stiffness and pulse pressure in hypertension and cardiovascular diseases. *Circulation, 107*(22), 2864–2869.

Safar, M. E., London, G. M., and Plante, G. E. (2004). Arterial stiffness and kidney function. *Hypertension, 43*(2), 163–168.

Safar, M. E. (2018). Arterial stiffness as a risk factor for clinical hypertension. *Nature Reviews. Cardiology, 15*(2), 97–105.

Safar, M. E., Asmar, R., Benetos, A., Blacher, J., Boutouyrie, P., Lacolley, P., ... and French Study Group on Arterial Stiffness. (2018). Interaction between hypertension and arterial stiffness: an expert reappraisal. *Hypertension*, *72*(4), 796–805.

Sakurai, M., Tetsu, Y., Hideshi, K., Kato, T., Kuroda, K., Ishisu, R., et al. (2007). The Relationship between Aortic Augmentation Index and Pulse Wave Velocity: An Invasive Study. *Journal of Hypertension, 25*(2), 391–397.

Schillaci, G., Bilo, G., Pucci, G., Laurent, S., Macquin-Mavier, I., Boutouyrie, P., et al. (2012). Relationship between short term blood pressure variability and large-artery stiffness in human hypertension: findings from 2 large databases. *Hypertension 60*, 369–377.

Segers, P., Rietzchel, E.R., Buyzere, M., de Bacquer, D., van Bortel, L.M., de Backer, G., et al. (2007). Assessment of Pressure Wave Reflection: Getting the Timing Right! *Physiological Measurement 28*, 1045–1056.

Segers, P., Rietzchel, E.R., de Buyzere, M.L., Vermeersch, S.J., de Bacquer, D., van Bortel, L.M., et al. (2007). Noninvasive (input) impedance, pulse wave velocity, and wave reflection in healthy middle-aged men and women. *Hypertension 49*, 1248–1255.

Segers, P., Rietzschel, E. R., and Chirinos, J. A. (2020). How to measure arterial stiffness in humans. *Arteriosclerosis, Thrombosis, and Vascular Biology, 40*(5), 1034–1043.

Sharman, J. E., Davies, J. E., Jenkins, C., and Marwick, T. H. (2009). Augmentation index, left ventricular contractility, and wave reflection. *Hypertension, 54*(5), 1099–1105.

Splansky, G. L., Corey, D., Yang, Q., Atwood, L. D., Cupples, L. A., Benjamin, E. J., ... & Levy, D. (2007). The third generation cohort of the National Heart, Lung, and Blood Institute's Framingham Heart Study: design, recruitment, and initial examination. *American Journal of Epidemiology*, *165*(11), 1328–1335.

Stauss H.M., Petitto C.E., Rotella D.L., Wong B.J., and Sheriff D.D. (2008). Very low frequency blood pressure variability is modulated by myogenic vascular function and is reduced in stroke patients. *Journal of Hypertension, 26*, 1127–1137.

Stergiopulos, N., Young, D., and Rogge, T. (1992). Computer simulation of arterial flow with applications to arterial and aortic stenoses. *Journal of Biomechanics, 25*(12), 1477–1488.

Stergiopulos, N., Westerhof, B. E., and Westerhof, N. (1999). Total arterial inertance as the fourth element of the windkessel model. *American Journal of Physiology. Heart and Circulatory Physiology, 276*(1), H81–88. https://doi.org/10.1152/ajpheart.1999.276.1.h81

Sugawara, J., Hayashi, K., Yokoi, T., Tanaka, H. (2008). Age-Associated Elongation of the Ascending Aorta in Adults. *JACC: Cardiovascular Imaging, 1*(6), 739–748.

Sun, Z. (2015). Aging, arterial stiffness, and hypertension. *Hypertension, 65*(2), 252–256.

Tanaka, H., and Safar, M. E. (2005). Influence of lifestyle modification on arterial stiffness and wave reflections. *American Journal of Hypertension, 18*(1), 137–144.

Taylor, M. G. (1959). An experimental determination of the propagation of fluid oscillations in a tube with a visco-elastic wall; together with an analysis of the characteristics required in an electrical analogue. *Physics in Medicine and Biology, 4*(1), 63–82.

Taylor, M. G. (1959). The influence of the anomalous viscosity of blood upon its oscillatory flow. *Physics in Medicine and Biology, 3*(3), 273–290.

Taylor, M.G. (1966). The Input Impedance of an Assembly of Randomly Branching Elastic Tubes. *Biophysical Journal, 6*(1), 29–51.

Theodor, M., Fiala, J., Ruh, D., Förster, K., Heilmann, C., Beyersdorf, F., et al. (2014). Implantable Accelerometer System for the Determination of Blood Pressure Using Reflected Wave Transit Time. *Sensors and Actuators A: Physical 206*, 151–158.

Tomita, H., Kawamoto, R., Tabara, Y., Miki, T., and Kohara, K. (2008). Blood pressure is the main determinant of the reflection wave in patients with type 2 diabetes. *Hypertension Research, 31*(3), 493–499.

Van den Wijngaard, J. P., Siebes, M., and Westerhof, B. E. (2008). Comparison of arterial waves derived by classical wave separation and wave intensity analysis in a model of aortic coarctation. *Medical & Biological Engineering & Computing, 47*(2), 211–220.

Van Varik, B.J., Rennenberg, R., Reutelingsperger, C.P., Kroon, A.A., de Leeuw, P.W., and Schurgers, L.J. (2012). Mechanisms of arterial remodeling: lessons from genetic diseases. *Frontiers in Genetics, 3*, 1–10.

Vlachopoulos, C., Xaplanteris, P., Aboyans, V., Brodmann, M., Cífková, R., Cosentino, F., et al. (2015). The role of vascular biomarkers for primary and secondary prevention. A position paper from the European Society of Cardiology Working Group on peripheral circulation: Endorsed by the Association for Research into Arterial Structure and Physiology (ARTERY) Society. *Atherosclerosis, 241*(2), 507–532.

Vliet, B. N., Chafe, L. L., and Montani, J. P. (2003). Characteristics of 24 h Telemetered Blood Pressure in eNOS-Knockout and C57Bl/6J Control Mice. T*he Journal of Physiology 1*, 313–325.

Vliet, B. N., McGuire, J., Chafe, L., Leonard, A., Joshi, A., and Montani, J.P. (2006). Phenotyping the level of blood pressure by telemetry in mice. *Clinical and Experimental Pharmacology and Physiology 11*, 1007–1015.

Volokh, K.Y. (2011). Modeling failure of soft anisotropic materials with application to arteries. *Journal of the Mechanical Behavior of Biomedical Materials, 4*(8), 1582–1592.

Weisbrod, R. M., Shiang, T., Al Sayah, L., Fry, J. L., Bajpai, S., Reinhart-King, C. A., ... & Seta, F. (2013). Arterial stiffening precedes systolic hypertension in diet-induced obesity. *Hypertension*, *62*(6), 1105–1110.

Westerhof, N., Bosman, F., De Vries, C. J., and Noordergraaf, A. (1969). Analog Studies of the human systemic arterial tree. *Journal of Biomechanics, 2*(2), 121–143.

Westerhof, N., and Noordergraaf, A. (1970). Arterial viscoelasticity: A generalized model. *Journal of Biomechanics, 3*(3), 357–379.

Westerhof, B.E., Westerhof, N. (2012). Magnitude and Return Time of the Reflected Wave. *Journal of Hypertension, 30*(5), 932–939.

Westerhof, B. E., and Westerhof, N. (2018). Uniform tube models with single reflection site do not explain aortic wave travel and pressure wave shape. *Physiological Measurement, 39*(12), 124006.

Westerhof, B. E., Van Gemert, M. J., and Van den Wijngaard, J. P. (2020). Pressure and flow relations in the systemic arterial tree throughout development from newborn

to adult. *Frontiers in Pediatrics, 8*(251).

Wilkinson, I. B., Fuchs, S. A., Jansen, I. M., Spratt, J. C., Murray, G. D., Cockcroft, J. R., & Webb, D. J. (1998). Reproducibility of pulse wave velocity and augmentation index measured by pulse wave analysis. *Journal of Hypertension, 16*(12), 2079–2084.

Wilkinson, I. B., MacCallum, H., Flint, L., Cockcroft, J. R., Newby, D. E., and Webb, D. J. (2000). The influence of heart rate on augmentation index and central arterial pressure in humans. *The Journal of Physiology, 525*(Pt 1), 263.

Wilkinson IB, Mohammad NH, Tyrrell S, Hall IR, Webb DJ, Paul VE, Levy T, Cockcroft JR. (2002). Heart rate dependency of pulse pressure amplification and arterial stiffness. *American Journal of Hypertension, 15*(1 Pt 1):24–30.

Wilkinson, I.B., Prasad, K., Hall, I.R., Thomas, A., MacCallum, H., Webb, D.J., et al. (2002). Increased Central Pulse Pressure and Augmentation Index in Subjects with Hypercholesterolemia. *Journal of the American College of Cardiology 39*, 1005–1011.

Williams, S. B., Cusco, J. A., Roddy, M. A., Johnstone, M. T., & Creager, M. A. (1996). Impaired nitric oxide-mediated vasodilation in patients with non-insulin-dependent diabetes mellitus. *Journal of the American College of Cardiology*, *27*(3), 567–574.

Womersley, J. R. (1957). Oscillatory flow in arteries: The constrained elastic tube as a model of arterial flow and Pulse Transmission. *Physics in Medicine and Biology, 2*(2), 178–187.

Xiao, H., Butlin, M., Tan, I., Avolio, A. (2017). Effects of Cardiac Timing and Peripheral Resistance on Measurement of Pulse Wave Velocity for Assessment of Arterial Stiffness. *Scientific Reports, 7*(1), 5990. https://doi.org/10.1038/s41598-017-05807-x

Xiao, H., Tan, I., Butlin, M., Li, D., Avolio, A. (2017). Arterial Viscoelasticity: Role in the Dependency of Pulse Wave Velocity on Heart Rate in Conduit Arteries. *American Journal of Physiology-Heart and Circulatory Physiology, 312*(6), H1185–H1194. https://doi.org/10.1152/ajpheart.00849.2016

Yambe, M., Tomiyama, H., Hirayama, Y., Gulniza, Z., Takata, Y., Koji, Y., et al. (2004). Arterial stiffening as a possible risk factor for both atherosclerosis and diastolic heart failure. *Hypertension Research, 27*, 625–631.

Yasmin, and Brown, M. J. (1999). Similarities and Differences between Augmentation Index and Pulse Wave Velocity in the Assessment of Arterial Stiffness. *QJM: Quarterly Journal of Medicine, 92*(10), 595–600.

Yoshimoto T., Eguchi, K., Sakurai, H., Ohmichi, Y., Hasimoto, T., Ohmichi, M., et al. (2011). Frequency components of systolic blood pressure variability reflect vasomotor and cardiac sympathetic functions in conscious rats. *Journal of Physiological Sciences, 61*, 373-383.

Zhang, Q., Suki, B., and Lutchen, K. R. (1995). Harmonic distortion from nonlinear systems with broadband inputs: applications to lung mechanics. *Annals of Biomedical Engineering, 23*, 672–681.

Zheng, X., Vieira Campos, A., Ordieres-Meré, J., Balseiro, J., Labrador Marcos, S., and Aladro, Y. (2017). Continuous monitoring of essential tremor using a portable system based on smartwatch. *Frontiers in Neurology, 8*, 96.

CURRICULUM VITAE